Journal of Medicinal Chemistry

Article

pubs.acs.org/jmc

Decreasing the Rate of Metabolic Ketone Reduction in the Discovery of a Clinical Acetyl-CoA Carboxylase Inhibitor for the Treatment of Diabetes

David A. Griffith,*[,†] Daniel W. Kung,*[,⊥] William P. Esler,[‡] Paul A. Amor,[‡] Scott W. Bagley,[⊥] Carine Beysen,[◆] Santos Carvajal-Gonzalez,[∥] Shawn D. Doran,[▽] Chris Limberakis,[⊥] Alan M. Mathiowetz,[†] Kirk McPherson,[#] David A. Price,[†] Eric Ravussin,[○] Gabriele E. Sonnenberg,[‡] James A. Southers,[⊥] Laurel J. Sweet,[#] Scott M. Turner,[◆] and Felix F. Vajdos[⊥]

[†]Worldwide Medicinal Chemistry, [‡]Cardiovascular, Metabolic and Endocrine Diseases Research Unit, and [∥]Clinical Research Statistics, Pfizer Worldwide Research and Development, Cambridge, Massachusetts 02139, United States

[⊥]Worldwide Medicinal Chemistry, [#]Cardiovascular, Metabolic and Endocrine Diseases Research Unit, and [▽]Pharmacokinetics, Dynamics and Metabolism, Pfizer Worldwide Research and Development, Groton, Connecticut 06340, United States

[○]Pennington Biomedical Research Center, Louisiana State University, Baton Rouge, Louisiana 70808, United States

[◆]KineMed, Inc., Emeryville, California 94608, United States

S *Supporting Information*

ABSTRACT: Acetyl-CoA carboxylase (ACC) inhibitors offer significant potential for the treatment of type 2 diabetes mellitus (T2DM), hepatic steatosis, and cancer. However, the identification of tool compounds suitable to test the hypothesis in human trials has been challenging. An advanced series of spirocyclic ketone-containing ACC inhibitors recently reported by Pfizer were metabolized in vivo by ketone reduction, which complicated human pharmacology projections. We disclose that this metabolic reduction can be greatly attenuated through introduction of steric hindrance adjacent to the ketone carbonyl. Incorporation of weakly basic functionality improved solubility and led to the identification of **9** as a clinical candidate for the treatment of T2DM. Phase I clinical studies demonstrated dose-proportional increases in exposure, single-dose inhibition of de novo lipogenesis (DNL), and changes in indirect calorimetry consistent with increased whole-body fatty acid oxidation. This demonstration of target engagement validates the use of compound **9** to evaluate the role of DNL in human disease.

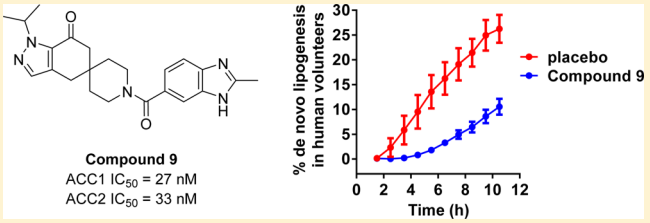

INTRODUCTION

Acetyl-CoA carboxylase (EC6.4.1.2) (ACC) is a biotin carboxylase that catalyzes the ATP-dependent condensation of acetyl-CoA and carbonate to form malonyl-CoA.[1] The malonyl-CoA produced by ACC serves two major physiologic functions. It is an essential and rate-limiting substrate for de novo lipogenesis (DNL), and it acts as an allosteric inhibitor of the enzyme carnitine-palmitoyl transferase I (CPT-1). CPT-1 is responsible for the transport of long-chain fatty acyl-CoAs across the mitochondrial membrane into the mitochondria where they become available for fatty acid oxidation. The transport step is rate-determining for this process. Thus, ACC is positioned as a key physiologic switch regulating the transition from oxidative to lipogenic metabolism. Metabolic perturbations, including suppressed fatty acid oxidation and increased hepatic DNL, have been hypothesized to contribute to ectopic accumulation of lipid species in muscle and liver, which in turn have been hypothesized to play a causative role in the molecular pathogenesis of insulin resistance.[2,3] Inhibition of malonyl-CoA production by ACC is expected to simultaneously inhibit DNL and increase flux through CPT-1, leading to increased β-oxidation of long-chain fatty acids, and thus may lead to reduced ectopic lipid accumulation and improved insulin sensitivity. ACC inhibition is therefore an attractive biological target for the treatment of metabolic diseases such as T2DM and nonalcoholic fatty liver disease.[4] Consistent with this hypothesis, antisense oligonucleotide inhibition of ACC significantly reduced diet-induced hepatic steatosis and hepatic insulin resistance.[5] The two closely related isoforms, ACC1 and ACC2, are encoded by separate gene products that differ in tissue and subcellular distribution.[1] ACC1 is primarily located in liver and adipose tissue, while ACC2 is the dominant isoform in skeletal and heart muscle. ACC1 is also expressed in multiple human cancers, making it an attractive oncology target.[6,7] We sought balanced inhibitors of ACC1 and ACC2 to gain benefit from inhibition of the enzyme in both liver and muscle.

Received: October 15, 2014
Published: November 25, 2014

   dx.doi.org/10.1021/jm5016022 | *J. Med. Chem.* 2014, 57, 10512−10526

Several ACC inhibitors have been disclosed in recent years, with much consideration directed toward understanding whether selective or balanced inhibition of ACC1/ACC2 is preferable. Published results to date have been controversial in terms of both efficacy and safety of the mechanism. Figure 1

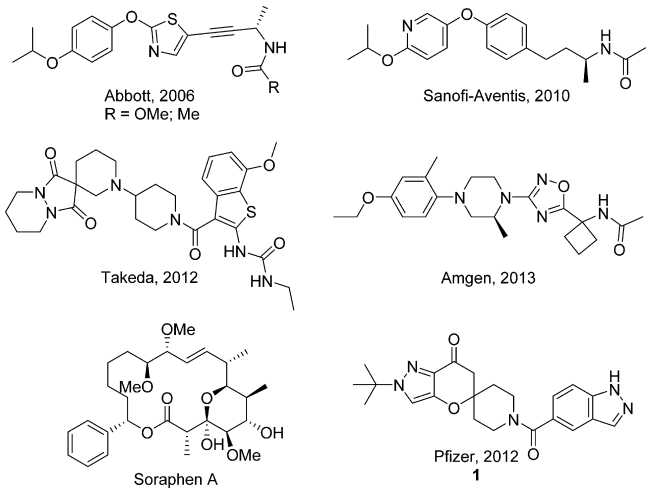

Figure 1. Literature ACC inhibitors.

highlights selected compounds with reported in vivo data. Abbott described an ACC2-selective thiazole ether (R = OMe) that elicited dose-dependent reductions in muscle malonyl-CoA levels.[8] However, significant neurological and cardiovascular safety events were observed and attributed to the alkyne-containing structure of the specific compound.[9] Using a related ACC2-selective compound from the Abbott disclosures (R = Me), Boehringer Ingelheim observed reductions in malonyl-CoA, stimulation of fatty acid oxidation, improvements in glucose tolerance, and HbA1c reductions following chronic treatment of db/db mice.[10] A phenyl ether from Sanofi-Aventis, with unselective activity against ACC1/ACC2, increased lipid oxidation but failed to decrease hepatic triglycerides or body weight in diet-induced obese (DIO) mice or in Zucker diabetic fatty rats after chronic administration.[11,12] Takeda described a spiro-pyrazolidinedione with balanced ACC1/ACC2 activity that showed dose-dependent changes in respiratory quotient in rats, providing evidence of increased fatty acid oxidation.[13,14] Amgen's piperazine oxadiazole with dual ACC1/ACC2 inhibition decreased malonyl-CoA levels but unexpectedly increased plasma glucose and impaired glucose tolerance in DIO mice treated for 28 days.[15] The natural product soraphen A, also an inhibitor of both ACC1/ACC2, decreased weight gain and body fat content in mice and improved insulin sensitivity, although a narrow safety window may have confounded the results.[16] Nimbus disclosed favorable impact on weight gain, triglycerides, cholesterol, and insulin sensitivity in DIO rats with a compound whose specific structure was not reported.[17,18] Pfizer described a spiroketone (**1**) that decreased malonyl-CoA in liver and muscle;[19] the subject of this paper is follow-up to that disclosure, along with preclinical and human biology data for a lead compound.

RESULTS AND DISCUSSION

Chemistry. The N2-alkyl pyrazole ketones with substitution at the α-position to the ketone and the N1-alkyl pyrazole ketones described in this work were synthesized by the general methods shown in Schemes 1 and 2. These synthetic routes have been described in detail previously.[20,21] The mono- and dimethyl substituted ketone cores in Scheme 1 were synthesized by α-alkylation of the respective precursor ketones. Although the desired enolates could be formed at low temperature by treatment of the ketone with lithium diisopropylamide (LDA) or lithium hexamethyldisilazide (LHMDS), the rate of alkylation (for example, with methyl iodide) was slow relative to the rate of ring-opening β-elimination of the oxy-pyrazole anion. Notably, addition of 1,3-dimethyl-3,4,5,6-tetrahydro-2(1*H*)-pyrimidinone (DMPU) achieved both increased efficiency of enolate formation and increased reactivity of the enolate to the desired alkylation. The pyrazoloketones in Scheme 2 were prepared by regioselective addition of alkyl hydrazines to a cyclohexenone intermediate, followed by functionalization of the olefin.

Biological Evaluation. Compound **1** was previously disclosed as a candidate for in vivo efficacy and toxicology evaluation,[19] demonstrating good potency against human ACC1 and ACC2 (IC_{50} = 111 and 9.8 nM, respectively) and low human liver microsomal clearance (<4.9 mL/min/kg). Key observations during the preparation for and analysis of those in vivo efficacy and safety studies guided the search for improved properties in subsequent compounds. First, during synthetic scale-up, a byproduct arising from ring-opening elimination of oxy-pyrazole was observed, presumably via a retro-Michael reaction analogous to that shown in Scheme 1, an obstacle that was overcome but which increased concern about potential instability of the β-pyrazoloxy-ketone functionality.[20] Second, crystalline compound **1** exhibited low solubility, requiring a spray-dried dispersion formulation to achieve adequate compound exposure in toxicology studies. Third, the ketone functional group in **1** was reduced in vivo to provide substantial circulating levels of the alcohol metabolite, **1m**.[22] The alcohol metabolite was formed upon incubation of **1** with rat, dog, and

Scheme 1. General Synthetic Route to N2-Alkyl Pyrazole Ketones with α-Methyl Substitution

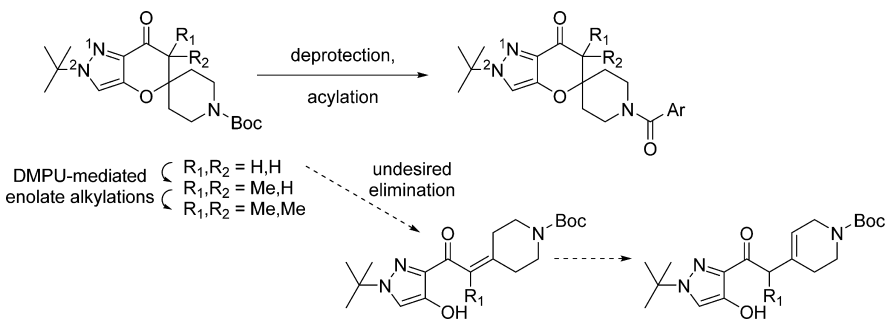

dx.doi.org/10.1021/jm5016022 | J. Med. Chem. 2014, 57, 10512−10526

Scheme 2. General Synthetic Route to N1-Substituted Pyrazole Ketones

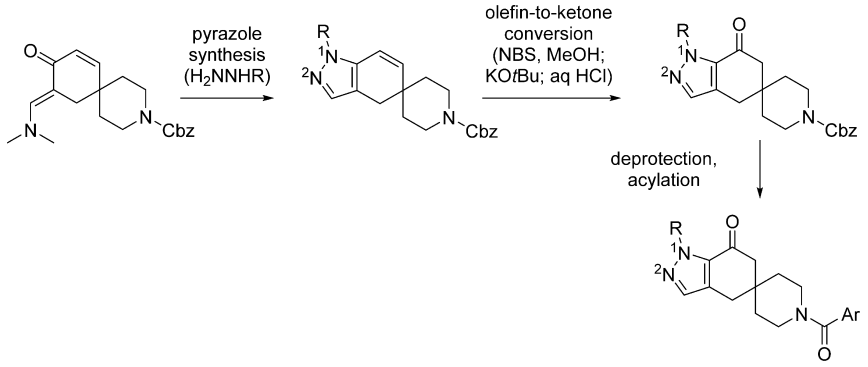

human liver microsomes, with reduction rates highest in dog and lowest in rat.[23] Pharmacokinetic (PK) studies in dog showed the alcohol metabolite **1m** had nine-times higher exposure relative to parent compound **1** (see Figure 2). The metabolite had substantially reduced ACC1 and ACC2 potency (IC_{50} = 8.7 and 1.0 μM, respectively; see Supporting Information, Table S1) relative to parent, but the high level of ketone reduction was a concern for two main reasons: (a) decreased confidence in human PK predictions with ketone reduction as a primary metabolic pathway and (b) increased off-target pharmacology risk due to high circulating levels of metabolite, with our attention focused primarily on hERG inhibition because ketone **1** and alcohol **1m** had similar potencies versus this ion channel (IC_{50} = 34 and 57 μM, respectively).

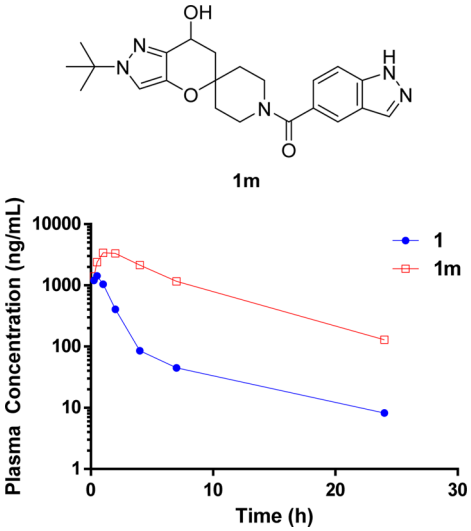

Figure 2. Plasma concentrations of **1** and its alcohol metabolite **1m** in beagle dogs following oral administration of **1** at 10 mg/kg. Metabolite **1m** had higher exposure ($AUC_{0-\infty}$ = 27800 ng·h/mL) than parent **1** ($AUC_{0-\infty}$ = 3030 ng·h/mL).

As a result of these observations from the study of compound **1**, a decreased rate of ketone reduction became the primary objective in the design of new compounds. The initial hypothesis for decreasing ketone reduction was to increase steric hindrance around the ketone,[24] leading to two approaches for substitution proximal to the ketone: adding alkyl substituents on the methylene adjacent to the ketone and altering the pyrazole to the regioisomeric N1-alkyl (rather than N2-alkyl) derivative.

Consideration of the crystal structure of **1** bound in ACC provided support for exploring the α-substitution strategy. As described previously,[25] the ACC CT-domain is an obligate homodimer, with the active site composed of residues from each monomer (denoted A and B). An X-ray cocrystal structure of **1** bound in a "humanized yeast" chimeric CT-domain of ACC[26] demonstrated binding to the putative biotin binding site consistent with previous structures (Figure 3).[25−27] Compound **1** bound in a generally hydrophobic cleft, with all of its polar atoms satisfied and sequestered from competing solvent interactions. The ketone and amide carbonyls made key hydrogen-bond contacts to the protein, orienting the rigid spirocycle in a low-energy conformation that allowed for ideal placement of polar and hydrophobic interactions with a minimal loss of conformational entropy. There appeared to be sufficient space adjacent to the ketone to accommodate substitution with alkyl groups, though specific interactions with the protein were not expected with small substituents. The probable impact of altering the pyrazole regioisomer was less clear. A crystallographic water was hydrogen-bonded to N1, but the water was calculated using HydroSite[28] to be low energy and easily displaced by a potential N1-substituent. However, there was also potential that the increased steric congestion would negatively impact the hydrogen-bond between the ketone and the backbone NH.

The results of introducing substituents on the carbon adjacent to the ketone are shown in Table 1. For routine screening, potencies were assessed versus human ACC1 and ACC2 using recombinant enzymes in a Transcreener format.[19] Consistent with the strategy employed in the identification of compound **1**, lipophilic efficiency (LipE) was a key parameter that was used to evaluate the quality of new compounds.[19] Unfortunately, the monomethyl stereoisomers, **2** and **3**, and the dimethyl derivative, **4**, demonstrated insufficient potency as ACC inhibitors. The additional lipophilicity relative to parent compound **1** also increased intrinsic clearance in human liver microsomes (hCL_{int}, Table 1). On the specific property of ketone reduction, the qualitative rate of ketone reduction as assessed by rate of alcohol formation in human liver microsomes was **1** > **2** ≈ **3** > **4** (data not shown). Evaluation of the dimethyl derivative **4** in a dog PK study (Figure 4) showed a marked decrease in the amount of alcohol metabolite **4m** relative to parent ketone (23-fold greater exposure for **4**). Although the α-alkylation approach did not seem likely to lead directly to a candidate, these ADME data provided strong

dx.doi.org/10.1021/jm5016022 | J. Med. Chem. 2014, 57, 10512−10526

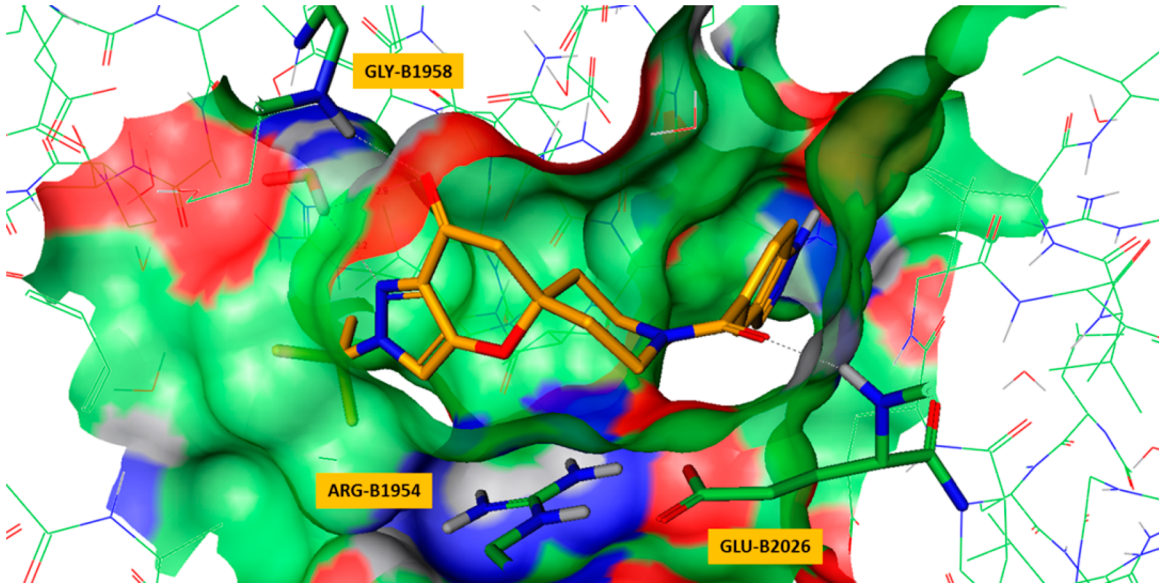

Figure 3. Co-crystal structure of **1** bound in the CT-domain binding domain of ACC. Compound **1** was oriented in the channel by hydrogen bonds between the ketone and NH-Gly-B1958 and between the amide carbonyl and NH-Glu-B2026. The pyrazolopyranone group was sandwiched in a hydrophobic cleft lined with side chains of Leu-A1762, Val-A1765, Leu-A1766, Ala-B1920, Val-B1923, and Phe-B1925. The hydrogen bonding potential of the pyranone ether oxygen was unsatisfied, but this region of the active site was capped by the side chain of Arg-B1954. The distance between the ether oxygen and the guanidinium group of the arginine (3.8 Å) was consistent with a weak electrostatic interaction, which likely alleviated the thermodynamic penalty associated with burying an unsatisfied hydrogen bonding group.

Table 1. N2-Substituted ACC Inhibitors[a]

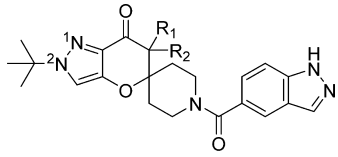

compd	R_1	R_2	eLogD[29]	hCL_{int} (mL/min/kg)	ACC1[b] IC_{50} (nM)	ACC1 LipE	ACC2[b] IC_{50} (nM)	ACC2 LipE	hERG IC_{50} (μM)
1	H	H	1.4	<4.9	111 (76−160)	5.6	9.8 (7.8−12)	6.6	34
2	Me	H	1.5	13	676 (347−1300)	4.6	63 (16−246)	5.6	ND
3	H	Me	1.5	20	674 (450−1000)	4.6	78 (31−200)	5.5	ND
4	Me	Me	1.8	42	3900 (2800−5400)	3.6	1100 (740−1600)	4.1	ND

[a]Human ACC1 and ACC2 potencies are the geometric mean of at least three replicates (95% confidence interval). hCL_{int} = intrinsic clearance in human liver microsomes; hERG = inhibition of the hERG channel in a patch-clamp assay; ND = not determined. [b]Transcreener assay.

support for the hypothesis that increased steric hindrance was a viable strategy for decreasing the rate of reduction.

The regioisomeric N1-alkyl pyrazole derivatives were the alternative structural change designed to increase steric hindrance around the ketone. The synthetic route developed for these compounds also provided the opportunity to replace the cyclic ether in compound **1** with a carbocycle, thus obviating the potential for retro-Michael ring-opening. The potency of the corresponding cyclic ether and carbocyclic analogues was similar for both the N2- and N1-alkyl series across a range of analogues (data not shown). Although there was some concern that removing the electron-donating ether might increase electrophilicity of the pyrazoloketone and the associated rate of ketone reduction, we believed that the steric effects of the N1-alkyl substituent would dominate any change in electronics.

The results of studies on N1-alkyl pyrazoles are shown in Table 2. Compounds **5**, **6**, and **7** with varying steric bulk of the N1-substituent showed an encouraging profile. Importantly, the structural changes from **1** to **5**/**6** retained both ACC potency and selectivity versus hERG. The relatively high LipE of compound **6**, which was reflected in the desirable balance of ACC potency and human liver microsomal (HLM) stability, led to selection of R = isopropyl as the preferred pyrazole N1-substituent. Having made structural changes to the core of the molecule that increased steric hindrance around the ketone and removed the potentially labile cyclic ether linkage, we focused on the piperidine amide group to improve solubility. Within the scope of 5,6-bicycloheteroaromatic groups (a topology found to be important for potency in the discovery of compound **1**), weakly basic rings were targeted to achieve the most desirable balance between solubility and hERG potency. Pyrrolopyridine **8** and benzimidazole **9** were two of the most promising derivatives, with the benzimidazole **9** favorably differentiating on both HLM stability and hERG activity. Furthermore, the solubility at pH 1.2 of crystalline compounds **8** (2320 μg/mL) and **9** (1980 μg/mL) increased substantially as compared to crystalline compound **1** (20 μg/mL). To assess the impact of pyrazole N1-substitution on the rate of ketone reduction, the benzimidazole **9** was tested in a dog PK study; the data

dx.doi.org/10.1021/jm5016022 | J. Med. Chem. 2014, 57, 10512−10526

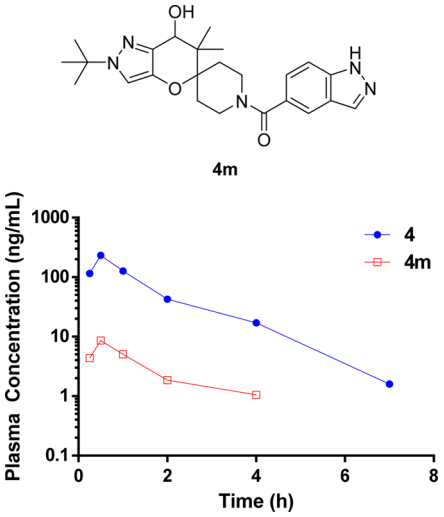

Figure 4. Plasma concentrations of **4** and its alcohol metabolite **4m** in beagle dogs following oral administration of **4** at 1 mg/kg. Metabolite **4m** had lower exposure ($AUC_{0-\infty}$ = 14 ng·h/mL) than parent **4** ($AUC_{0-\infty}$ = 321 ng·h/mL).

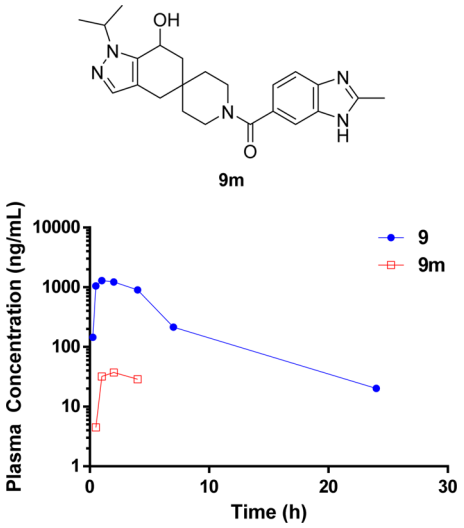

Figure 5. Plasma concentrations of **9** and its alcohol metabolite **9m** in beagle dogs following oral administration of **9** at 3 mg/kg. Plasma levels of **9m** were below the lower level of quantitation beyond the 4 h time point. Metabolite **9m** had lower exposure ($AUC_{0-\infty}$ = 330 ng·h/mL) than parent **9** ($AUC_{0-\infty}$ = 7930 ng·h/mL).

depicted in Figure 5 demonstrated a 24-fold lower exposure to alcohol metabolite **9m** as compared to parent compound **9**.

Comparison of the X-ray cocrystal structures of **1** and **6** bound in the CT-domain of ACC showed that both inhibitors maintained hydrogen bonds between the two carbonyls and protein backbone NHs (Figure 6). As predicted, the N1 substituent of **6** displaced the crystallographic water that was hydrogen-bonded to the ketone and to the pyrazole N1 in the bound structure of **1**. Notably, however, the pyrazoloketone group of compound **6** shifted by ∼17° relative to **1** such that the N1-*i*Pr group bound in a similar position to the N2-*t*Bu group. The concomitant shift in the ketone position resulted in a less favorable geometry but a nearly identical hydrogen bond length for **6** as compared to **1**, suggesting comparable binding energies for the two interactions. The piperidine and indazole groups were essentially undisturbed by the N1 substitution and made similar interactions with the protein as in the structure of **1**.

Compound **9** met our initial project objectives with its attractive overall profile of ACC inhibitory potency, relatively low extent of ketone reduction, increased solubility, diminished hERG activity, and good HLM stability. Described below is further in vitro and in vivo characterization of this compound.

The preclinical pharmacokinetic properties of **9** are summarized in Table 3. Compound **9** exhibited low protein binding in both rat and dog plasma but approximately 10-fold higher binding in both monkey and human plasma. The in vitro metabolism of **9** was evaluated in microsomes from rat, dog, and human hepatocytes. Compound **9** was not metabolized (as assessed by disappearance of parent) in rat, dog, or human microsomes. Compound **9** was also stable in human hepatocyte incubations (data not shown), but was minimally metabolized by recombinant human CYP3A4 and CYP3A5, suggesting it is a substrate for CYP3A4 and CYP3A5.

In vivo, the plasma clearance of **9** was low following intravenous (iv) administration (1 mg/kg) to rats, dogs, and monkeys (Table 4). Oral (po) administration (3 mg/kg) to rats and dogs showed bioavailability of 40% and 54%, respectively, consistent with the low microsomal clearance and good solubility at low pH. The bioavailability following a 50 mg/kg oral dose in rats was 106%, suggesting saturation of clearance.

A 96-well radioenzymatic assay using both recombinant human and purified rat ACC isozymes was used to confirm in vitro inhibitory potency for the determination of pharmacokinetic/pharmacodynamic (PK/PD) relationships. This assay format was also used with recombinant human ACC2 to

Table 2. N1-Substituted ACC Inhibitors[a]

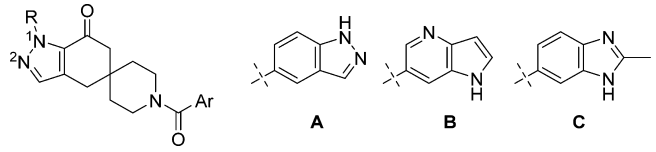

compd	R	Ar	eLogD[29]	hCL_{int} (mL/min/kg)	ACC1[b] IC_{50} (nM)	ACC1 LipE	ACC2[b] IC_{50} (nM)	ACC2 LipE	hERG IC_{50} (μM)
5	*t*Bu	A	2.8	20	40 (24–66)	4.6	17 (12–25)	5.0	21
6	*i*Pr	A	2.0	<10	62 (35–110)	5.2	30 (21–41)	5.5	23
7	Et	A	1.4	12	317 (110–940)	5.1	161 (88–290)	5.4	ND
8	*i*Pr	B	1.8	26	41 (15–110)	5.6	23 (15–35)	5.8	29
9	*i*Pr	C	1.9	<4.9	98 (56–170)	5.1	45 (27–74)	5.5	141

[a]Human ACC1 and ACC2 potencies are the geometric mean of at least three replicates (95% confidence interval). [b]Transcreener assay.

dx.doi.org/10.1021/jm5016022 | J. Med. Chem. 2014, 57, 10512–10526

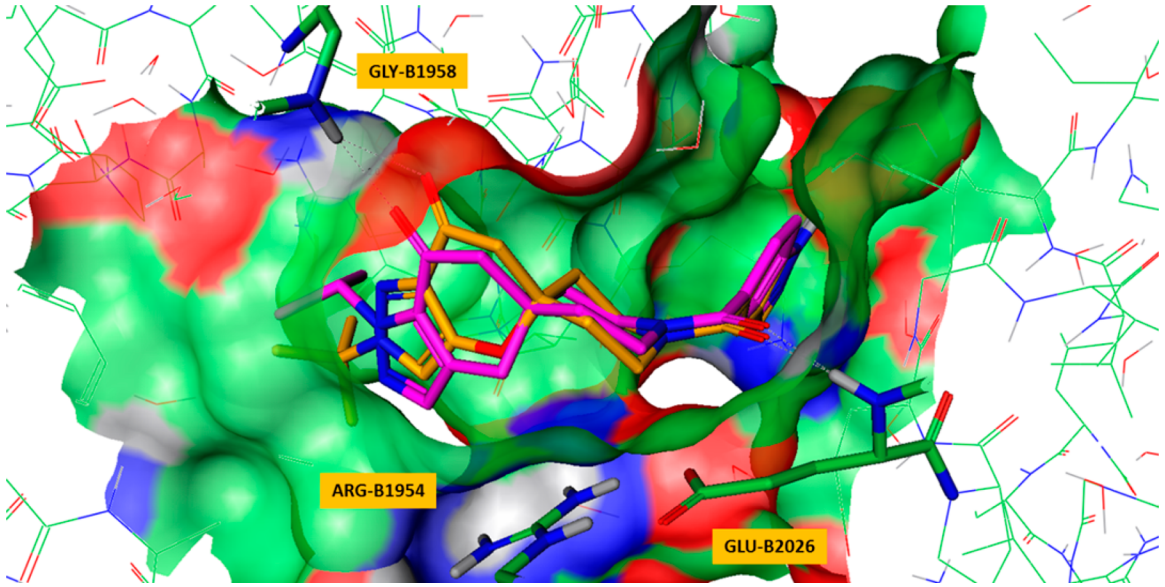

Figure 6. Co-crystal structure of **6** (magenta) bound in the CT-domain of ACC, overlaid with the bound conformation of **1** (orange).

Table 3. Pharmacokinetic Parameters of 9

	rat	dog	monkey	human
PPB[a] (% unbound)	24	34	2.4	1.3
microsomes	rat	dog	monkey	human
CL_{int} (mL/min/kg)	<21	<8	ND	<4.9
Predicted CL_h[b]	<8	<5	ND	<0.1

in vivo	rat			dog		monkey
dose	1[c]	3[d]	50[d]	1[e]	3[f]	1[g]
route	iv	po	po	iv	po	iv
AUC_{exp} (ng·h/mL)	686	825	36400	4990	8020	7270
CL (mL/min/kg)	25	NA	NA	3.4	NA	2.4
V_{ss} (L/kg)	1.5	NA	NA	0.77	NA	0.19
$T_{1/2}$ (h)	2.3	4.8	2.3	5.0	5.7	2.9
F (%)	NA	40	106	NA	54	NA

[a]Plasma protein binding. [b]CL_h microsomes estimated from well-stirred model, including blood:plasma ratio and plasma and microsomal binding. [c]Fed, vehicle: 20% SBECD. [d]Fed, vehicle: 0.5% methocellulose/0.1% tween80. [e]Fed, vehicle: 40% 2-pyrrolidinone/60% pH 4.5 citrate buffer, solution, sterile filtered, pH = 5.41. [f]Fed, vehicle: 0.5% methyl cellulose, suspension, pH = 6.4. [g]Fed, Vehicle: 10% DMSO/20% 2-pyrrolidinone/70% of 20% SBECD in water.

Table 4. Summary of Key Pharmacologic Properties of 9[a]

in vitro assays	IC_{50} or EC_{50} (nM)
human ACC1 enzyme assay[b]	27.0 ± 2.7
human ACC2 enzyme assay[b]	33.0 ± 4.1
rat ACC1 enzyme assay[b]	23.5 ± 1.1
rat ACC2 enzyme assay[b]	50.4 ± 2.6
inhibition of malonyl-CoA in primary rat hepatocytes	29.9 ± 7.4

in vivo assays	ED_{50} (mg/kg)	EC_{50} (unbound plasma drug concentration) (nM)
inhibition of hepatic malonyl-CoA in rats	6.0	540
inhibition of skeletal muscle malonyl-CoA in rats	11	870
inhibition of hepatic DNL in rats	7.8	326
respiratory exchange ratio lowering in rats	3.5	119

[a]In vitro potencies are the geometric mean of at least 3 replicates ± the standard error of the mean (SEM). [b]Radiometric assay.

determine the mode and reversibility of inhibition. Compound **9** was found to be uncompetitive with ATP and noncompetitive with carbonate and acetyl-CoA (see Lineweaver–Burk plots in the Supporting Information), consistent with previously reported inhibitors binding in this pocket of the protein.[4] Dose–response experiments were performed at saturating concentrations of ATP and acetyl-CoA where the inhibitory concentration (IC_{50}) approximated the equilibrium dissociation constant for an enzyme (K_i) for uncompetitive inhibitors. Compound **9** was shown to inhibit both rat and human ACC1 and ACC2 in vitro with similar potencies (Table 4 and Supporting Information). The human ACC1 and ACC2 potencies in the radiometric assays were 3- and 2-fold more potent, respectively, than values determined in the Transcreener assays.

Ex vivo, the effect of **9** on the ACC/malonyl-CoA axis was assessed in primary rat hepatocytes (Figure 7). Compound **9** inhibited formation of malonyl-CoA in a concentration-

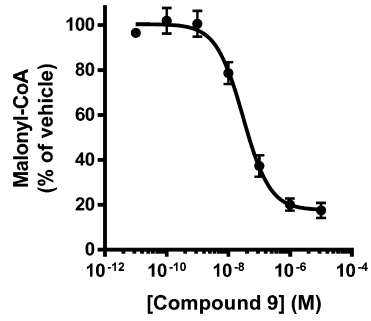

Figure 7. Effect of **9** on malonyl-CoA levels in primary rat hepatocytes. Data shown represent the mean of seven independent experimental studies. Cryopreserved rat hepatocytes were plated on collagen-coated 96-well plates and overlaid with matrigel. The cultured hepatocytes were incubated in the presence and absence of a range of concentrations of **9**. Following incubation, malonyl-CoA levels in lysates from the treated and untreated hepatocytes were analyzed using high-throughput mass spectrometry.

dx.doi.org/10.1021/jm5016022 | J. Med. Chem. 2014, 57, 10512–10526

dependent manner with a potency (EC_{50} = 30 nM) in rat hepatocytes consistent with its potency against rat ACC1 (24 nM).

On the basis of the robust enzyme and cellular activity of **9**, the effects of the compound on modulation of ACC activity in vivo was assessed first as changes in levels of malonyl-CoA, and subsequently as the downstream impact on DNL and fuel substrate utilization. The low plasma clearance and high exposure following oral administration in rats (see Table 3) enabled the ready examination of in vivo pharmacology.

Formation of the direct product of ACC, malonyl-CoA, in the skeletal muscle (quadriceps) and liver of lean Sprague–Dawley (SD) rats was assessed 1 h following an acute oral dose of **9**, showing concentration-dependent reductions in both skeletal muscle and liver malonyl-CoA (Figure 8). At the nadir,

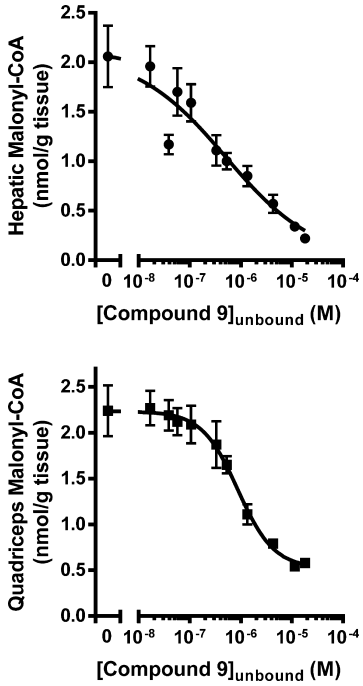

Figure 8. Free plasma concentration–effect relationship of orally dosed **9** and malonyl-CoA tissue levels in liver and quadriceps from male SD rats. Rats were dosed by oral gavage with vehicle or a range of doses of **9**. One hour postdose, rats were euthanized, plasma was collected for compound exposure measurements, and liver and skeletal muscle (quadriceps) were rapidly removed and freeze-clamped in liquid nitrogen. Malonyl-CoA content of tissue extracts was determined by liquid chromatography mass spectrometry (LC-MS). Tissue concentrations of malonyl-CoA for each dose group were plotted against the corresponding free plasma concentrations of **9** measured from the same animals.

quadriceps and liver malonyl-CoA levels were reduced by 76% and 89%, respectively. The EC_{50}s for inhibition of quadriceps and liver malonyl-CoA were 870 and 540 nM, respectively, determined from unbound plasma concentrations of **9**.

To confirm that the observed malonyl-CoA biomarker reduction led to the anticipated changes in lipid metabolism, we examined the impact of **9** on DNL and respiratory exchange ratio (RER), the latter being an indication of whole-body fuel substrate utilization. Acute oral administration of **9** inhibited hepatic DNL in rats in an unbound plasma drug concentration-dependent manner. Compound **9** inhibited up to 82% of the incorporation of [^{14}C]acetate into [^{14}C]lipids with an EC_{50} of 326 nM (Figure 9).

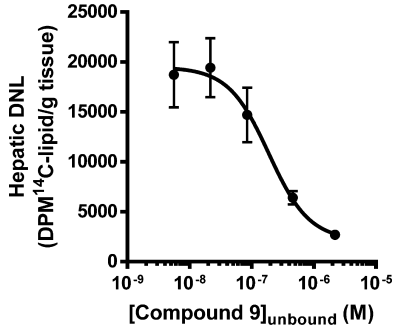

Figure 9. Free plasma concentration–effect relationship of orally dosed **9** and DNL. Lean, male SD rats fed ad libitum with standard chow were dosed by oral gavage with vehicle or a range of doses of **9**. One hour postdose, animals were injected intraperitoneally with [^{14}C]acetate. One hour later, animals were euthanized and liver punch samples and plasma were collected. The [^{14}C]lipid generated from the [^{14}C]acetate through DNL was isolated and measured from the liver samples by organic extraction with ethanol and petroleum ether and quantified by scintillation counting. Compound exposure was assessed in plasma samples from the same animals.

Consistent with the role of ACC in modulating fatty acid oxidation, oral treatment with **9** also produced acute reductions in whole-body RER. To drive the basal fuel substrate utilization toward increased dependence on carbohydrate usage (increased RER), rats were fasted for 24 h and then re-fed a high sucrose diet for 48 h prior to the experiment. Following baseline RER measurement, the rats were dosed by oral gavage with a range of doses of **9** or vehicle. Immediately following dosing, animals were returned to the metabolic chambers and RER was monitored for an additional 105 min. Following the last RER measurement, animals were euthanized and skeletal muscle and plasma were collected for malonyl-CoA and drug exposure measurements, respectively.

Within 15 min of oral administration of **9**, dose-dependent reductions in RER indicated a shift in fuel substrate utilization toward increased net whole-body dependence on fatty acid utilization (Figure 10a). At the nadir, RER values in the highest two doses of **9** dropped 0.19 units and at 120 min postdose the EC_{50} was 119 nM (Figure 10b). Further, the change in RER from predose was found to be proportional to the quadriceps malonyl-CoA levels measured from the same animals (Figure 10c).

Overall, the mechanistic studies with compound **9** in rats demonstrated that decreases in liver and skeletal muscle malonyl-CoA lead to downstream decreases in DNL and increases in the use of fatty acids as fuel substrate. Secondary in vitro pharmacology studies did not identify any significant off-target activity for **9**. In vivo safety pharmacology studies of **9** were conducted in rat and dog; doses with no observed adverse effects were identified in both species.

Human Clinical Evaluations. The effects described above for liver and muscle malonyl-CoA, DNL, and RER in rats were the foundation for a rat PK/PD model that was then applied to predict human dosing for **9**. Quadriceps muscle malonyl-CoA level (QMCoA) in rat was chosen as the primary mechanistic biomarker. On the basis of the rapid formation and elimination (seconds to min) of malonyl-CoA in muscle tissue, a direct response model was selected as a reasonable approximation to

dx.doi.org/10.1021/jm5016022 | J. Med. Chem. 2014, 57, 10512–10526

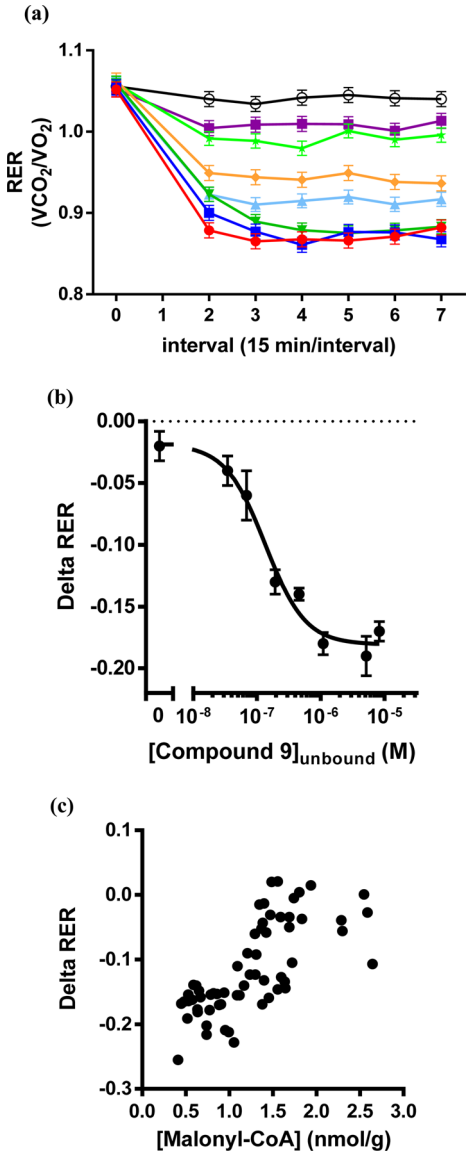

Figure 10. Respiratory exchange ratio (RER) in male SD rats dosed orally with **9**. (a) Time course of individual treatment groups. Rats were treated with a single oral dose of **9** at 100 mg/kg (red circle), 40 mg/kg (blue square), 20 mg/kg (green inverted triangle), 10 mg/kg (light-blue triangle), 5 mg/kg (orange diamond), 2 mg/kg (green star), 1 mg/kg (purple square), or vehicle (black open circle) at time zero, immediately following the baseline measurement period shown. RER was measured for an additional 105 min after dosing. Following completion of the final RER period, the rats were euthanized. Quadriceps were collected and freeze-clamped for quantification of malonyl-CoA levels; plasma was collected for drug exposure measurements. (b) Unbound plasma concentration-change in RER relationship at steady state following treatment. (c) Relationship between quadriceps malonyl-CoA levels and change in RER measured in the same animal.

describe the PK/PD relationship. Using the resulting rat QMCoA PK/PD model and the predicted human PK of **9**, GastroPlus was used to project the steady-state dose necessary to achieve 50% inhibition of human quadriceps ACC2 at the steady-state average concentration (C_{ave}). These projections, after correction for species differences in ACC2 enzyme potency (radiometric assay) and plasma/tissue protein binding, were based on assumptions of: (a) a 1:1 translation in QMCoA response between rats and humans, and (b) as observed in rat, a 1:1 relationship between human free muscle and free plasma drug concentrations. On the basis of these assumptions and models, the clinical plasma concentration of **9** to achieve 50% inhibition of human quadriceps ACC2 was predicted to be 14800 ng/mL (473 nM free), which would be achieved by a dose of 125 mg once-daily.

In the First-in-Human study, the safety, tolerability, and pharmacokinetics of single doses of **9** were tested according to a randomized, placebo-controlled, double-blind, parallel-group design. Seven sequential cohorts of healthy volunteers were randomized to receive either **9** or placebo (six and three subjects per cohort, respectively). Compound **9** was administered at escalating doses ranging from 10 to 800 mg; the 800 mg dose was provided as split doses of 400 mg in the a.m. and p.m.

Overall, single ascending doses of **9** were safe and well-tolerated, exhibiting a benign adverse event profile similar to placebo-treated subjects. Five adverse events were considered to be potentially treatment related, including nightmare in two subjects [one treated with placebo and one with **9** (800-mg split dose)], gastroesophageal reflux disease in one subject treated with **9** (300 mg), dyspepsia in one subject treated with **9** (600 mg), and dry mouth in one subject treated with **9** (300 mg). All potentially treatment-related adverse events were mild in intensity. In the fasted state, rapid absorption was noted with median peak concentrations observed 1−2 h postdose (Figure 11). The pharmacokinetic profiles exhibited low-to-moderate

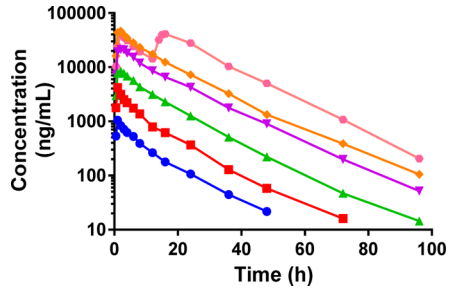

Figure 11. Time-course of plasma concentration of **9** in healthy human volunteers at a range of doses. Compound **9** was administered orally at 10 (blue circles), 30 (red squares), 100 (green triangles), 300 (purple triangles), 600 (orange circles), and 800 (as 2 × 400, pink circles) mg doses.

interindividual variability in AUC and C_{max}. AUC was approximately proportional to dose over the 10−800 mg range, while C_{max} was observed to be slightly less than dose-proportional. Dosing in the presence of food (300 mg dose) resulted in a delayed T_{max} (3.5 h), with marginal differences in peak and total exposure. Terminal half-life values were consistent across doses and were independent of dosing in the presence of food, with mean values of 10−13 h (data not shown).

The pharmacodynamic effects of **9** on metabolic parameters were evaluated at the top (nonsplit) dose in a double-blinded, placebo-controlled crossover study in healthy volunteers in each of two study periods. Hepatic DNL was assessed by measuring the incorporation of ^{13}C-labeled acetate into very low density lipoprotein triglyceride (VLDL-TG), quantified using mass isotopomer distribution analysis (MIDA).[30] Whole-body fuel substrate utilization was assessed by measuring RER using indirect calorimetry. Subjects were randomized to receive

dx.doi.org/10.1021/jm5016022 | J. Med. Chem. 2014, 57, 10512−10526

a single oral dose of **9** (600 mg) or placebo in the first period and were crossed over to receive the other treatment at least 1 week apart. Oral fructose loading was used during the 10 h duration of DNL and RER assessments to provide reproducible fractional contribution of DNL to VLDL-TG[31] as well as elevated and reproducible RER measures from one assessment period to the other.

Oral fructose administration increased the fractional contribution of DNL over fasting values to a peak fractional DNL contribution of approximately 27% (Figure 12a). In

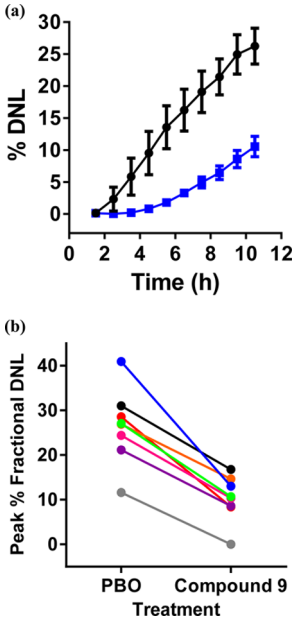

Figure 12. (a) Fructose-stimulated fractional DNL in subjects treated with placebo (PBO, black circles) or a single dose of compound **9** (600 mg, blue squares) using a crossover design. (b) Treated subjects had significantly lower peak fractional DNL (10.5%; 90% CI = 7.6−13.5%) compared with placebo (26.5%; 90% CI = 20.9−32.1%). All data were corrected for baseline DNL.

subjects treated with compound **9**, fructose stimulated DNL was inhibited over this time course; peak fructose-stimulated fractional DNL was reduced by 63.6% (90% CI = 75.1−52.0%) relative to placebo treatment. All subjects responded to treatment with similar reductions in peak fractional DNL (Figure 12b). The observed DNL reductions were consistent with preclinical dose and concentration projections. Further details will be provided in due course.

The effect of **9** on RER was assessed by indirect calorimetry in the same subjects concurrent with the above DNL determinations. Over the course of the study, the $AUC_{0.5-10h}$ for RER values in subjects treated with **9** were significantly lower than for subjects treated with placebo (ratio = 0.86, 90%; CI 0.81−0.92), indicating an increase in net whole-body fatty acid utilization in the **9** subjects compared with placebo subjects (Figure 13).

CONCLUSION

The design, synthesis, and biological characterization of a dual ACC1/ACC2 inhibitor with low clearance and high off-target selectivity have been described. Metabolic ketone reduction was greatly attenuated through introduction of steric hindrance adjacent to the ketone carbonyl. Phase I clinical studies

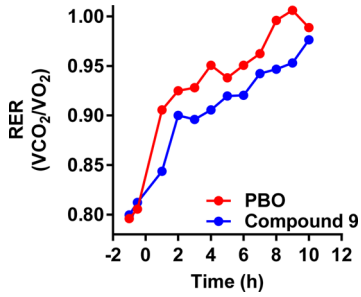

Figure 13. Baseline corrected respiratory exchange ratio (RER) over time in subjects treated by crossover design with placebo or a single dose of compound **9** (600 mg). Curves represent median data from the subjects. Treated subjects had significantly lower RER compared with placebo.

demonstrated dose-proportional increases in exposure, a pharmacokinetic profile suitable for once-daily dosing, single-dose inhibition of DNL, and increased net whole-body fatty acid utilization that support its further clinical evaluation in type 2 diabetes patients.

EXPERIMENTAL SECTION

General Experimental Methods. All chemicals, reagents, and solvents were purchased from commercial sources and used without further purification. ^{1}H NMR spectra are reported relative to residual solvent signals. Data for ^{1}H NMR spectra are reported as follows: chemical shift (δ ppm), multiplicity, coupling constant (Hz), and integration. The multiplicities are denoted as follows: s, singlet; d, doublet; t, triplet; q, quartet; sept, septet; m, multiplet; (v) br s, (very) broad singlet; app, apparent. Silica gel chromatography was performed using a medium pressure Biotage or ISCO system and columns prepackaged by various commercial vendors including Biotage and ISCO. Whatman precoated silica gel plates (250 μm) were used for analytical thin-layer chromatography (TLC). The terms "concentrated" and "evaporated" refer to the removal of solvent at reduced pressure on a rotary evaporator with a water bath temperature not exceeding 60 °C. Purity of final compounds was assessed by reversed-phase HPLC with UV detection at 215 nM; all tested compounds were >95% purity, unless otherwise noted.

*(2′-(tert-Butyl)-7′-hydroxy-6′,7′-dihydro-2′H-spiro[piperidine-4,5′-pyrano[3,2-c]pyrazol]-1-yl)(1H-indazol-5-yl)methanone (**1m**).* Sodium borohydride (0.37 g, 10 mmol, 2.5 equiv) was added to a suspension of 2′-(*tert*-butyl)-1-(1*H*-indazole-5-carbonyl)-2′*H*-spiro-[piperidine-4,5′-pyrano[3,2-*c*]pyrazol]-7′(6′*H*)-one[19] (1.67 g, 4.10 mmol, 1 equiv) in methanol (24 mL). After 1 h, the mixture was partitioned between water and ethyl acetate (2×). The combined organic layers were washed sequentially with water and with brine, and the organics were dried over sodium sulfate, filtered, and concentrated to afford a foam that was triturated with ether to afford an off-white solid that was dried under vacuum (1.0 g, 67%). ^{1}H NMR (400 MHz, DMSO-d_6) δ 13.19 (s, 1H), 8.10 (br s, 1H), 7.82 (s, 1H), 7.54 (d, J = 8.6 Hz, 1H), 7.36 (s, 1H), 7.36 (dd, J = 8.6, 1.2 Hz, 1H), 5.19 (d, J = 5.4 Hz, 1H), 4.66 (app q, J = 5.5 Hz, 1H), 4.08 (v br s, 1H), 3.51 (br s, 1H), 3.23 (br s, 2H), 1.98 (dd, J = 14.1, 5.9 Hz, 1H), 1.91 (br s, 1H), 1.81 (dd, J = 14.1, 6.1 Hz, 1H), 1.70 (m, 3H), 1.42 (s, 9H). +ESI MS (M + H) 410.2.

*Enantiomers of 2′-(tert-Butyl)-1-(1H-indazole-5-carbonyl)-6′-methyl-2′H-spiro[piperidine-4,5′-pyrano[3,2-c]pyrazol]-7′(6′H)-one (**2** and **3**).* A solution of hydrogen chloride in dioxane (4M, 3 mL, 12 mmol, 12 equiv) was added to a solution of *tert*-butyl 2′-(*tert*-butyl)-6′-methyl-7′-oxo-6′,7′-dihydro-2′*H*-spiro[piperidine-4,5′-pyrano[3,2-*c*]pyrazole]-1-carboxylate[21] (400 mg, 1.1 mmol, 1 equiv) in dioxane (4 mL). After 2 h, the mixture was concentrated and the residue was triturated with ether. The resulting solid was partitioned between aqueous sodium hydroxide solution (3 mL) and ethyl acetate (2 × 3 mL). The combined organics were dried over magnesium sulfate,

dx.doi.org/10.1021/jm5016022 | J. Med. Chem. 2014, 57, 10512−10526

filtered, and concentrated to afford the amine as an oil (215 mg, 65%), which was used without further purification.

A solution of 1*H*-indazole-5-carboxylic acid (111 mg, 0.69 mmol, 1.0 equiv), 2-chloro-4,6-dimethoxy-1,3,5-triazine (120 mg, 0.69 mol, 1.0 equiv), and *N*-methylmorpholine (0.15 mL, 1.4 mmol, 2.0 equiv) in DMF (2 mL) was stirred for 1 h, then a solution of 2′-(*tert*-butyl)-6′-methyl-2′*H*-spiro[piperidine-4,5′-pyrano[3,2-*c*]pyrazol]-7′(6′*H*)-one (215 mg, 0.69 mmol, 1 equiv) in DMF (3 mL) was added and the resulting solution was stirred for another 2 h. The product mixture was partitioned between saturated aqueous ammonium chloride solution (25 mL) and ethyl acetate (2 × 15 mL). The combined organics were concentrated, and the resulting residue was purified by column chromatography twice, first using 4% methanol in dichloromethane as eluent, then using 50−100% ethyl acetate in heptanes, to afford the racemic product (144 mg, 50%). The enantiomers were separated by SFC (Chiralpak AD-H, 65:35 CO_2:methanol) to afford compounds **2** (retention time 3.61 min, 51 mg, 18%, chiral purity >99%) and **3** (retention time 5.63 min, 40 mg, 14%, chiral purity >99%). **2**: ^{1}H NMR (400 MHz, DMSO-d_6) δ 13.21 (s, 1H), 8.12 (s, 1H), 7.84 (s, 1H), 7.77 (s, 1H), 7.55 (d, J = 8.5 Hz, 1H), 7.38 (d, J = 8.5 Hz, 1H), 4.30 (v br s, 1H), 3.59 (v br s, 1H), 3.19 (v br s, 2H), 2.61 (q, J = 7.0 Hz, 1H), 1.90 (br s, 2H), 1.70 (m, 2H), 1.49 (s, 9H), 1.06 (d, J = 7.0 Hz, 3H); +ESI MS (M + H) 422.4. **3**: ^{1}H NMR (400 MHz, DMSO-d_6) δ 13.21 (s, 1H), 8.12 (s, 1H), 7.84 (s, 1H), 7.77 (s, 1H), 7.55 (d, J = 8.5 Hz, 1H), 7.38 (d, J = 8.5 Hz, 1H), 4.29 (v br s, 1H), 3.60 (v br s, 1H), 3.19 (v br s, 2H), 2.61 (q, J = 7.0 Hz, 1H), 1.89 (br s, 2H), 1.71 (m, 2H), 1.49 (s, 9H), 1.06 (d, J = 7.0 Hz, 3H); +ESI MS (M + H) 422.2. The purity of compound **3** was 92% (HPLC, UV 215 nM).

*2′-(tert-Butyl)-1-(1H-indazole-5-carbonyl)-6′,6′-dimethyl-2′H-spiro[piperidine-4,5′-pyrano[3,2-c]pyrazol]-7′(6′H)-one (**4**).* A solution of hydrogen chloride in dioxane (4M, 0.86 mL, 3.5 mmol, 15 equiv) was added to a solution of *tert*-butyl 2′-(*tert*-butyl)-6′,6′-dimethyl-7′-oxo-6′,7′-dihydro-2′*H*-spiro[piperidine-4,5′-pyrano[3,2-*c*]-pyrazole]-1-carboxylate[21] (90 mg, 0.23 mmol, 1 equiv) in dioxane (2.5 mL). After 18 h, the mixture was concentrated and the resulting residue was concentrated from heptanes. The resulting solid (81 mg) was used without further purification.

A solution of 1*H*-indazole-5-carboxylic acid (40 mg, 0.25 mmol, 1.0 equiv), 2-chloro-4,6-dimethoxy-1,3,5-triazine (43 mg, 0.25 mol, 1.0 equiv), and *N*-methylmorpholine (82 μL, 0.74 mmol, 3.0 equiv) in DMF (3 mL) was stirred for 1 h, then a solution of 2′-(*tert*-butyl)-6′,6′-dimethyl-2′*H*-spiro[piperidine-4,5′-pyrano[3,2-*c*]pyrazol]-7′(6′*H*)-one hydrochloride (81 mg, 0.25 mmol, 1 equiv) in DMF (3 mL) and *N*-methylmorpholine (54 μL, 0.50 mmol, 2.0 equiv) were added sequentially and the resulting solution was stirred for another 1.5 h. The product mixture was diluted with saturated aqueous ammonium chloride solution (1 mL), and the resulting mixture was partitioned between water (5 mL) and ethyl acetate (30 mL + 20 mL). The combined organics were dried over magnesium sulfate, filtered, and concentrated. Purification of the residue by column chromatography (0−5% methanol in dichloromethane) afforded the product as a solid (74 mg, 69%). ^{1}H NMR (400 MHz, DMSO-d_6) δ 13.19 (s, 1H), 8.10 (br s, 1H), 7.84 (s, 1H), 7.76 (s, 1H), 7.54 (app d, J = 8.6 Hz, 1H), 7.38 (dd, J = 8.1, 1.6 Hz, 1H), 4.32 (v br s, 1H), 3.84 (br s, 1H), 3.12 (v br s, 2H), 1.84 (m, 2H), 1.73 (m, 2H), 1.48 (s, 9H), 1.07 (s, 6H). +ESI MS (M + H) 436.6.

*(2′-(tert-Butyl)-7′-hydroxy-6′,6′-dimethyl-6′,7′-dihydro-2′H-spiro-[piperidine-4,5′-pyrano[3,2-c]pyrazol]-1-yl)(1H-indazol-5-yl)-methanone (**4m**).* Sodium borohydride (11 mg, 0.28 mmol, 1.1 equiv) was added to *tert*-butyl 2′-(*tert*-butyl)-6′,6′-dimethyl-7′-oxo-6′,7′-dihydro-2′*H*-spiro[piperidine-4,5′-pyrano[3,2-*c*]pyrazole]-1-carboxylate[21] (100 mg, 0.26 mmol, 1 equiv) in methanol (2 mL) at 0 °C. After 1 h at ambient temperature, the mixture was again cooled to 0 °C and an additional portion of sodium borohydride was added (10 mg, 0.26 mmol, 1.0 equiv). After an additional 2 h at ambient temperature, the mixture was cooled to 0 °C and water (1 mL) was added. The mixture was concentrated, and the resulting residue was partitioned between water (5 mL) and ethyl acetate (2 × 30 mL). The combined organic layers were dried over sodium sulfate, filtered, and concentrated to afford a solid (98 mg, 98%), which was used without further purification.

A solution of hydrogen chloride in dioxane (4 M, 1.8 mL, 7.2 mmol, 30 equiv) was added to a solution of *tert*-butyl 2′-(*tert*-butyl)-7′-hydroxy-6′,6′-dimethyl-6′,7′-dihydro-2′*H*-spiro[piperidine-4,5′-pyrano[3,2-*c*]pyrazole]-1-carboxylate (95 mg, 0.24 mmol, 1 equiv) in dioxane (2 mL). After 6 h, the mixture was concentrated to afford an oil which was used without further purification.

A solution of 1*H*-indazole-5-carboxylic acid (39 mg, 0.24 mmol, 1.0 equiv), 2-chloro-4,6-dimethoxy-1,3,5-triazine (43 mg, 0.24 mol, 1.0 equiv), and *N*-methylmorpholine (80 μL, 0.73 mmol, 3.0 equiv) in DMF (5 mL) was stirred for 1 h, then a solution of 2′-(*tert*-butyl)-6′,6′-dimethyl-6′,7′-dihydro-2′*H*-spiro[piperidine-4,5′-pyrano[3,2-*c*]-pyrazol]-7′-ol hydrochloride (80 mg, 0.24 mmol, 1 equiv) in DMF (3 mL) and *N*-methylmorpholine (52 μL, 0.50 mmol, 2.0 equiv) were added sequentially and the resulting solution was stirred for another 18 h. The product mixture was diluted with saturated aqueous ammonium chloride solution (3 mL), and the resulting mixture was partitioned between water (10 mL) and ethyl acetate (2 × 50 mL). The combined organics were dried over magnesium sulfate, filtered, and concentrated. Purification of the residue by column chromatography (0−8% methanol in dichloromethane) afforded the product as a solid (67 mg, 63%). ^{1}H NMR (400 MHz, DMSO-d_6) δ 13.19 (s, 1H), 8.10 (br s, 1H), 7.82 (s, 1H), 7.53 (d, J = 8.6 Hz, 1H), 7.36 (dd, J = 8.6, 1.6 Hz, 1H), 7.35 (s, 1H), 5.25 (d, J = 6.3 Hz, 1H), 4.30 (v br s, 1H), 4.19 (br s, 1H), 3.60 (v br s, 1H), 3.09 (v br s, 2H), 1.99 (br s, 1H), 1.68 (m, 3H), 1.42 (s, 9H), 0.89 (br s, 6H). +ESI MS (M + H) 438.5.

*1-(tert-Butyl)-1′-(1H-indazole-5-carbonyl)-1,4-dihydrospiro-[indazole-5,4′-piperidin]-7(6H)-one (**5**).* A suspension of 1-(*tert*-butyl)-1,4-dihydrospiro[indazole-5,4′-piperidin]-7(6*H*)-one hydrochloride[32] (158 mg, 0.53 mmol, 1 equiv), 1*H*-indazole-5-carboxylic acid (86 mg, 0.53 mmol, 1.0 equiv), HATU (207 mg, 0.53 mmol, 1.0 equiv), and triethylamine (0.15 mL, 1.1 mmol, 2.0 equiv) were combined in DMF (7 mL) and stirred at room temperature for 16 h. The mixture was partitioned between water (5 mL) and ethyl acetate (3 × 15 mL). The combined organics were washed sequentially with saturated aqueous sodium bicarbonate solution (5 mL) and brine (5 mL). After concentration, the resulting residue was partitioned between dichloromethane (20 mL) and 10% aqueous citric acid solution (5 mL) to remove residual triethylamine hydrochloride. The organic layer was dried over magnesium sulfate, filtered, and concentrated. The resulting residue was purified by column chromatography (3−8% methanol in dichloromethane) to afford the title compound as a solid (69 mg, 32%). ^{1}H NMR (400 MHz, $CDCl_3$) δ 10.23 (br s, 1H), 8.10 (s, 1H), 7.82 (br s, 1H), 7.49 (d, J = 8.6 Hz, 1H), 7.43 (dd, J = 8.6, 1.4 Hz, 1H), 7.29 (s, 1H), 3.46 (m, 4H), 2.81 (s, 2H), 2.61 (s, 2H), 1.64 (s, 9H), 1.57 (m, 4H). +APCI MS (M + H) 406.3.

*1′-(1H-Indazole-5-carbonyl)-1-isopropyl-1,4-dihydrospiro-[indazole-5,4′-piperidin]-7(6H)-one (**6**).* 1-Isopropyl-1,4-dihydrospiro[indazole-5,4′-piperidin]-7(6*H*)-one hydrochloride[20] (30.3 g, 94.6 mmol, 1 equiv) and 1*H*-indazole-5-carboxylic acid (16.96 g, 104.6 mmol, 1.1 equiv) were suspended in *N*,*N*-dimethylacetamide (430 mL) and 1-ethyl-3-[3-(dimethylamino)-propyl]carbodiimide hydrochloride (22.3 g, 115 mmol, 1.2 equiv) was added, followed by the dropwise addition of triethylamine (65 mL, 475 mmol, 5.0 equiv). 1-Hydroxybenzotriazole hydrate (16.2 g, 106 mmol, 1.1 equiv) was then added, and the reaction mixture was stirred at 60 °C for 2 h. The reaction was poured into half-saturated aqueous ammonium chloride solution (500 mL) and extracted with ethyl acetate (1 × 1 L, 2 × 500 mL). The combined organic layers were washed with aqueous sodium bicarbonate solution (2 × 500 mL), water (3 × 500 mL), and aqueous saturated sodium chloride solution (500 mL). The organic layer was dried over sodium sulfate, filtered, and concentrated under reduced pressure to an oil. The oil was purified via column chromatography (1−6% methanol in dichloromethane) to afford the desired product (27.1 g). A small amount was crystallized from ethyl acetate/heptanes, which was then used to seed the following crystallization. The product was dissolved in ethyl acetate

dx.doi.org/10.1021/jm5016022 | J. Med. Chem. 2014, 57, 10512−10526

(100 mL) and heated to reflux until the solution turned hazy. A small amount of seed crystal was added. The mixture was cooled to room temperature, and a precipitate formed and was stirred for 80 h. The precipitate was collected by filtration and washed with cold ethyl acetate (2 × 30 mL). The material was air-dried and then further dried under high vacuum to afford an off-white solid (23 g, 62%). ^{1}H NMR (400 MHz, DMSO-d_6) δ 13.19 (s, 1H), 8.10 (m, 1H), 7.79 (m, 1H), 7.53 (m, 1H), 7.43 (s, 1H), 7.34 (m, 1H), 5.24 (sept, J = 6.6 Hz, 1H), 3.45 (v br s, 4H), 2.78 (s, 2H), 2.59 (s, 2H), 1.48 (br s, 4H), 1.32 (d, J = 6.6 Hz, 6H). +ESI MS (M + H) 392.5.

*1-Ethyl-1′-(1H-indazole-5-carbonyl)-1,4-dihydrospiro[indazole-5,4′-piperidin]-7(6H)-one (**7**).* A mixture of benzyl 1-ethyl-7-oxo-1,4,6,7-tetrahydrospiro[indazole-5,4′-piperidine]-1′-carboxylate[20] (358 mg, 0.97 mmol, 1 equiv) and palladium on carbon (50% wet, 60 mg) in ethanol (20 mL) was treated with 50 psi hydrogen gas for 4 h. The mixture was filtered through Celite, rinsing with ethanol (50 mL). The filtrate was concentrated, then the resulting residue was slurried in heptanes (20 mL) and concentrated. The resulting solid was dissolved in dichloromethane (5 mL) and was treated with triethylamine (0.40 mL, 2.9 mmol, 3.0 equiv) and 1*H*-indazole-5-carbonyl chloride (211 mg, 0.97 mmol, 1.0 equiv) for 18 h at ambient temperature. The mixture was partitioned between water (50 mL) and ethyl acetate (2 × 50 mL). The combined organics were dried over sodium sulfate, filtered, and concentrated. Purification by column chromatography (2−10% methanol in dichloromethane) afforded the title compound as a solid (172 mg, 47%). ^{1}H NMR (400 MHz, $CDCl_3$) δ 8.13 (s, 1H), 7.85 (s, 1H), 7.51 (d, J = 8.6 Hz, 1H), 7.46 (d, J = 8.6 Hz, 1H), 7.37 (s, 1H), 4.52 (q, J = 7.2 Hz, 2H), 3.64 (v br s, 4 H), 2.82 (s, 2H), 2.61 (s, 2H), 1.63 (br s, 4H), 1.40 (t, J = 7.2 Hz, 3H). +ESI MS (M + H) 378.2.

*1-Isopropyl-1′-(1H-pyrrolo[3,2-b]pyridine-6-carbonyl)-1,4-dihydrospiro[indazole-5,4′-piperidin]-7(6H)-one (**8**).* A suspension of 1-isopropyl-1,4-dihydrospiro[indazole-5,4′-piperidin]-7(6*H*)-one hydrochloride[20] (100 mg, 0.35 mmol, 1 equiv), 1*H*-pyrrolo[3,2-*b*]pyridine-6-carboxylic acid (57 mg, 0.35 mmol, 1.0 equiv), HATU (83 mg, 0.35 mmol, 1.0 equiv), and triethylamine (0.10 mL, 0.70 mmol, 2.0 equiv) were combined in DMF (3 mL) and stirred at room temperature for 16 h. The mixture was partitioned between saturated aqueous sodium bicarbonate solution (10 mL) and ethyl acetate (2 × 5 mL). The combined organics were washed sequentially with water (5 mL) and brine (5 mL). After concentration, the resulting residue was purified by column chromatography (5% methanol in ethyl acetate) to afford the title compound as a solid (65 mg, 47%). ^{1}H NMR (400 MHz, DMSO-d_6) δ 11.76 (br s, 1H), 8.43 (d, J = 1.8 Hz, 1H), 7.95 (br s, 1H), 7.86 (t, J = 2.9 Hz, 1H), 7.46 (s, 1H), 6.65 (m, 1H), 5.27 (sept, J = 6.6 Hz, 1H), 3.56 (m, 4H), 2.82 (s, 2H), 2.63 (s, 2H), 1.53 (m, 4H), 1.36 (d, J = 6.6 Hz, 6H). +APCI MS (M + H) 392.2.

*1-Isopropyl-1′-(2-methyl-1H-benzo[d]imidazole-6-carbonyl)-1,4-dihydrospiro[indazole-5,4′-piperidin]-7(6H)-one (**9**).* *N*,*N*-Dimethylformamide (0.33 mL, 4.3 mmol, 0.05 equiv) and oxalyl chloride (22.1 mL, 257 mmol, 3.0 equiv) were added to a solution of 2-methyl-1*H*-benzimidazole-5-carboxylic acid (15 g, 85 mmol, 1 equiv) in tetrahydrofuran (500 mL). The reaction solution was stirred at ambient temperature for 16 h. The solution was concentrated, and the resulting residue was twice taken up in dichloromethane and concentrated under reduced pressure. To the resulting acid chloride was added tetrahydrofuran (500 mL), 1-isopropyl-1,4-dihydrospiro-[indazole-5,4′-piperidin]-7(6*H*)-one hydrochloride[20] (25.9 g, 91 mmol, 1.1 equiv), and triethylamine (71.2 mL, 510 mmol, 6.0 equiv). The solution was stirred at room temperature for 16 h, then saturated aqueous sodium bicarbonate solution (250 mL) was added and the resulting mixture was stirred for 5 min. The layers were separated, and the aqueous layer was extracted with 1:1 ethyl acetate−tetrahydrofuran. The organic layers were combined, diluted with ethyl acetate (1 L), and washed sequentially with saturated aqueous sodium bicarbonate solution (200 mL) and saturated aqueous sodium chloride solution. The organic layer was dried over sodium sulfate, filtered, and concentrated to afford a light-yellow solid. The solid was dissolved in hot methanol (300 mL) and then heated to reflux. To the solution was added 350 mL of ethyl acetate, and 300 mL of solvent was then removed by distillation. Additional ethyl acetate was added dropwise until an internal temperature of 70 °C was reached. The solution was cooled to ambient temperature over 3 h. The resulting solids were collected by filtration and dried in a vacuum oven (40 °C) for 16 h to afford a white solid (20.5 g, 59%). ^{1}H NMR (400 MHz, DMSO-d_6) δ 12.29 (br s, 1H), 7.43 (m, 3H), 7.11 (m, 1H), 5.24 (sept, J = 6.5 Hz, 1H), 3.45 (m, 4H), 2.77 (s, 2H), 2.57 (s, 2H), 2.45 (s, 3H), 1.46 (m, 4H), 1.32 (d, J = 6.5 Hz, 6H). +ESI MS (M + H) 406.5.

*(7-Hydroxy-1-isopropyl-1,4,6,7-tetrahydrospiro[indazole-5,4′-piperidin]-1′-yl)(2-methyl-1H-benzo[d]imidazol-6-yl)methanone (**9m**).* Sodium borohydride (27 mg, 0.76 mmol, 2.2 equiv) was added to 1-isopropyl-1′-(2-methyl-1*H*-benzo[*d*]imidazole-6-carbonyl)-1,4-dihydrospiro[indazole-5,4′-piperidin]-7(6*H*)-one (139 mg, 0.34 mmol, 1 equiv) in methanol. After 1 h, water (1 mL) was added dropwise and the resulting mixture was partitioned between ethyl acetate (20 mL) and water. The organic layer was washed with brine, dried over sodium sulfate, and concentrated. The resulting solid was purified by column chromatography (2−20% methanol in dichloromethane) to afford a white solid (75 mg, 54%). ^{1}H NMR (400 MHz, DMSO-d_6) δ 12.32 (br s, 1H), 7.43 (m, 2H), 7.13 (s, 1H), 7.11 (dd, J = 8.2, 1.6 Hz, 1H), 5.19 (d, J = 6.6 Hz, 1H), 4.71 (m, 2H), 3.47 (v br s, 4H), 2.46 (s, 3H), 2.41 (d, J = 15.3 Hz, 1H), 2.32 (d, J = 15.3 Hz, 1H), 1.96 (dd, J = 13.4, 5.8 Hz, 1H), 1.66 (dd, J = 13.4, 6.8 Hz, 1H), 1.56 (br s, 1H), 1.43 (m, 3H), 1.34 (d, J = 6.4 Hz, 3H), 1.28 (d, J = 6.6 Hz, 3H). +ESI MS (M + H) 408.3.

X-ray Crystallography. The preparation and crystal structure analysis of "humanized" ACC CT domain has been described previously.[26] Compounds **1** or **6** were soaked for 24 h into humanized ACC CT domain crystals at a concentration of 3 mM, then flash cooled in liquid propane prior to data collection. Data for compound **1** was collected at beamline X29A at the National Synchrotron Light Source (Brookhaven National Laboratory, Upton, NY, USA). Data for compound **6** was collected at sector 17BM of the Industrial Macromolecular Crystallography Association Collaborative Access Team (IMCA-CAT) (Advanced Photon Source, Argonne, IL). Data were processed using the programs AutoPROC and XDS.[33,34] All data handling was performed with programs from the CCP4 suite.[35−37] The structures of ACC-CT were determined by rigid body refinement of a reference structure against the isomorphous data. Compound **1** was refined using the program AUTOBUSTER;[38] compound **6** was refined using REFMAC.[39] Data and refinement statistics are reported in Table 5.

Transcreener ACC Inhibition Assay Description. Recombinant human ACC1[40] (rhACC1) was utilized in enzyme inhibition assays as previously described.[27] Recombinant human ACC2[27] (rhACC2) was prepared, purified, and utilized in enzyme inhibition assays as previously described.[27]

Radiometric ACC Inhibition Assay Description. Rat ACC1 and ACC2 were purified from rat liver and muscle, respectively, as previously described.[4] Enzyme inhibition assays were performed as previously described.[19]

Malonyl-CoA Production Inhibition in Rat Hepatocytes. Cryopreserved male Wistar rat hepatocytes from Xenotech were thawed and isolated using a percol rat hepatocyte isolation kit. Hepatocytes were plated in seeding media containing high glucose DMEM, 5% FBS, 1 μM dexamethasone, 4 μg/mL insulin, 1% pen/strep, and 1% glutamine. Hepatocytes were plated in 48-well collagen coated type I plates using a viable seeding density of 125000 cells/well in seeding media to result in 80−90% confluency at 5% CO_2 and 37 °C. Media was aspirated 4−6 h later and fresh Hepatocyte Modified Eagle Medium, Dr. Chee's Modification (MCM) was added. Fresh cold MCM media containing a 1:40 dilution of Matrigel, 250 ng/mL, 200 μL/well was added 24 h post seeding. The assay was run 72 h post seeding with a MCM media change the night before the experiment.

On the day of the study, media was aspirated and cells were treated with fresh MCM media containing DMSO vehicle or varying concentrations of **9** as indicated. Compound was initially dissolved in DMSO and subsequently diluted 1:100 in MCM. An aliquot of this solution was added to the fresh MCM in each well, further diluting the

Table 5. Crystallographic Data and Refinement Statistics

compd	1	6
(A) Data Collection		
space group	$P2_12_12_1$	$P2_12_12_1$
unit cell	a = 94.4	a = 94.5
	b = 137.8	b = 138.0
	c = 184.6	c = 184.8
resolution (Å)	42−2.89	110−2.23
(high res)	(3.04−2.89)	(2.35−2.23)
completeness (%)	90.2 (92.6)	98.1 (99.1)
R_{sym} [a]	0.114 (0.489)	0.077 (0.497)
redundancy	5.4 (5.3)	5.0 (4.9)
$\langle I\rangle/\langle\sigma(I)\rangle$	12.5 (3.2)	14.4 (2.9)
(B) Refinement		
R_{work} [b]	0.154	0.177
R_{free} [b]	0.207	0.209
protein atoms (no.)	11578	11149
waters (no.)	547	1521
average B_{Wilson} (Å^2)	60.5	38.1
average B (Å^2)	47.4	41.8
RMSD bond length (Å)	0.01	0.01
RMSD angles (deg)	1.19	1.11
Ramachandran (%) [c]	99.4	99.1
Ramachandran outliers (%)	0.6	0.9

[a] $R_{sym} = \sum_{hkl}(|I_{hkl} - \langle I_{hkl}\rangle|)/\sum_{hkl}\langle I_{hkl}\rangle$, where I_{hkl} is the intensity of reflection hkl, and $\langle I_{hkl}\rangle$ is the average intensity of multiple observations. [b] $R_{work} = \sum|F_o - F_c|/\sum F_o$, where F_o and F_c are the observed and calculated structure factor amplitudes, respectively. R_{free} is the R-factor for a randomly selected 5% of reflections which were not used in the refinement. [c] %(preferred) + %(allowed)

compound by 1:10. This dilution progression ensured that all wells had a final DMSO concentration of 0.1%. After 5 h at 37 °C, incubation media was removed and the experiment was terminated by washing the cells with ice-cold PBS. Cells were lysed with the addition of 70 μL of 10% trichloroacetic acid (TCA). Plates were mixed for 20 min at 4 °C and centrifuged at 2200*g* for 5 min. Supernatant (48 μL) was transferred to a ScreenMates Clear 384 Well V Bottom polypropylene microplates and frozen. Malonyl-CoA concentration was measured using RapidFire mass spectrometry analysis. TCA, ammonium acetate, methanol, acetone, acetonitrile, and water were used to make the necessary mobile phases. Adenosine 5′-triphosphate disodium salt hydrate (ATP) was used for sample preparation. Rapidfire Type D Hypercarb cartridges were obtained from BioCius. Samples were provided as 48 μL in 10% TCA. Then 2 μL of malonyl-$^{13}C_3$-CoA internal standard (0.4 pmol/μL final) and 2 mM final ATP in 10% TCA were added to the reaction and mixed. The samples were analyzed on a RapidFire platform coupled to a Sciex API4000 triple quadrupole mass spectrometer (RF-MS). Malonyl-CoA and malonyl-$^{13}C_3$-CoA were monitored in positive ion mode following MRM transitions at 854.1/347.1 and 857.1/350.1, respectively. Sample (10 μL) was aspirated directly from assay plates quenched with TCA (10% final). The aspirated sample was loaded onto the RF MS microscale solid-phase Hypercarb extraction cartridge (D) and washed with HPLC grade H_2O in a 3 s wash cycle to remove the nonvolatile assay components. The product and internal standard were coeluted to the mass spectrometer in 3 s with 50% H_2O, 25% MeCN, 25% acetone, and 5 mM ammonium acetate. Ion chromatograms were integrated using the Rapidfire Integrator software. Peak area ratios (malonyl-CoA/malonyl-$^{13}C_3$-CoA) were compared against a standard curve prepared in 10% aqueous TCA to determine sample concentrations of malonyl-CoA. Malonyl-CoA values were expressed as pmol/μL and compared against a standard curve. Dose response curves of malonyl-CoA inhibition by ACC inhibitor compound **9** were generated by plotting percent of control. An average EC_{50} was determined from seven independent experiments.

Malonyl-CoA Production Inhibition in Rats. Male SD rats were weighed and randomized by body weight into treatment groups consisting of vehicle, 0.25, 0.5, 1, 2, 4, 8, 15, 25, 50, and 100 mg/kg of **9**. Immediately prior to initiation of the study, the dosing solutions were prepared in dosing vehicle (0.5% methyl cellulose:0.1% polysorbate 80), giving a final dosing volume of 5 mL/kg. Animals were orally dosed 2 h into the light cycle with their respective treatments and fed ad libitum. One hour postdose, the animals were sacrificed via CO_2 asphyxiation followed by cervical dislocation. Blood for plasma exposure of compound **9** was collected via cardiac puncture, transferred to BD Microtainers tubes with K_2EDTA, centrifuged at 4 °C, and the plasma transferred to a 96-well microtiter plate and stored at −20 °C. Liver and quadriceps were rapidly removed, freeze-clamped in a Wollenberg clamp (precooled in liquid nitrogen), and subsequently stored at −80 °C.

Approximately 200 mg of pulverized tissue were added to the lysing matrix tube (MP Bio, Lysing matrix tube A for quadriceps and Lysing matrix tube D for liver) containing ice-cold 10% TCA, giving a final ratio of 1:5, tissue to acid. Samples were immediately pulverized using Fast Prep FP-120 (MP Bio). The extracted samples were then centrifuged at 4 °C and 20000*g* for 15 min (liver) and 30 min (muscle).

The supernatants containing malonyl-CoA were frozen at −80 °C until analysis was completed via LC-MS MS using an ABI Sciex API-3000 triple quadrupole mass spectrometer with turbo ion spray. Tissue concentrations for malonyl-CoA were calculated from a standard curve prepared in a 10% solution of TCA in water and ranged from 0.01 to 1 pmol/μL. Malonyl-$^{13}C_3$-CoA (final concentration of 0.4 pmol/μL) was added to each standard curve component and served as an internal standard, and the resulting chromatograms were integrated using Analyst software (Applied Biosystems).

DNL Inhibition in Rats. This procedure was derived from a published method for the examination of rat liver de novo lipid synthesis.[4] On the day of the study, male SD rats, previously randomized into groups of seven based on body weight, were administered a single dose of compound **9** or vehicle via oral gavage 2 h into the light cycle (8 a.m.). [2-^{14}C]-Acetic acid (Amersham) was diluted to 64 μCi/mL with saline prior to being administered intraperitoneally at 2.5 mL/kg 1 h postdose of compd/vehicle. Then 1 h following ^{14}C-acetic acid administration, the animals were sacrificed (CO_2 euthanasia) and liver samples collected (~400 mg, bifurcated median lobe) using disposable tissue biopsy punches. Analysis of DNL in these samples was performed as previously described.[4]

Briefly, tissues were saponified in aqueous NaOH (1.5 mL of 2.5 M). Following complete degradation, absolute ethanol (2.5 mL) was added to each sample and vigorously mixed. The samples were extracted with petroleum ether (4.8 mL). Following centrifugation to separate the organic and aqueous phases, the upper organic phase was removed and discarded. Concentrated HCl (0.6 mL of 12 M) was added to the remaining aqueous phase and vortexed vigorously. The acidified aqueous phase was subsequently extracted with petroleum ether (4.8 mL) and then centrifuged to separate the organic and aqueous phases. The upper organic phase was collected in an appropriately sized scintillation vial. The remaining aqueous phase was extracted with petroleum ether as described above, and the organic phase was combined with the previous extract. The combined organic phases were evaporated to dryness under gentle flow of nitrogen at room temperature. Compatible scintillation fluid was added to each vial, and the level of ^{14}C in the extraction was determined.

The data were analyzed with Microsoft Excel and plotted using GraphPad Prism 5. Statistical analysis (one-way ANOVA, Dunnett's posttest) was performed using GraphPad Prism 5.

RER Studies in Rats. Male SD rats were fasted for 24 h and then re-fed a diet high in sucrose (D10001, Research Diets) for 2 days prior to study initiation to elevate baseline respiratory exchange ratio (RER). On the day of experiment, rats were removed from their home cage, weighed, and individually placed into the calibrated indirect calorimetery chambers (Oxymax, Columbus Instruments, Columbus, OH) with free access to water and diet (D10001). Baseline oxygen consumption and carbon dioxide production rates were measured

dx.doi.org/10.1021/jm5016022 | J. Med. Chem. 2014, 57, 10512−10526

every 15 min for 75 min before treatment. After collecting baseline calorimetery data, rats were dosed orally with either vehicle control (0.5% methylcellulose/0.1% tween 80) or **9** (1, 2, 5, 20, 40, or 100 mg/kg) and then returned to the calorimetry chambers. Oxygen consumption and carbon dioxide production were measured for an additional 2.25 h after being placed back in the calorimetry chamber. Immediately following completion of the calorimetry measurement period, the animals were sacrificed by CO_2 asphyxiation followed by cervical dislocation. Plasma for determining plasma exposure of compound **9** was collected via cardiac puncture, and quadriceps muscles were rapidly removed, freeze-clamped as described above, and stored at −80 °C. Quadriceps malonyl-CoA content was measured as described above.

DNL and RER Studies in Humans. Studies involving human subjects were conducted in compliance with the ethical principles originating in or derived from the Declaration of Helsinki and in compliance with all International Conference on Harmonisation (ICH) Good Clinical Practice (GCP) Guidelines. In addition, all local regulatory requirements were followed, in particular, those affording greater protection to the safety of trial participants. Final study protocols and informed consent document were reviewed and approved by the investigational centers participating in the studies and by an independent Institutional Review Board (IRB). The investigator was required to inform the IRB of the study's progress and occurrence of any serious and/or unexpected adverse events. A signed and dated informed consent was required before any screening procedures were initiated. The investigator or his/her delegate explained the nature, purpose, and risks of the study to each subject. Each subject was informed that he/she could withdraw from the study at any time and for any reason. Each subject was given sufficient time to consider the implications of the study before deciding whether to participate. Subjects who chose to participate signed an informed consent document.

Safety, tolerability, and pharmacokinetics were evaluated in the first-in-human study. A total of 63 healthy volunteers (all male; mean age 32.6 years [range 20−45 years]; mean body mass index (BMI) 27.0 kg/m^2; [range 21.3−35.1 kg/m^2]) participated in the study. Seven sequential cohorts of volunteers were randomized to receive either **9** or placebo (six and three per cohort, respectively). Compound **9** was administered at escalating doses ranging from 10 to 800 mg; the 800 mg dose was provided as split doses of 400 mg in the a.m. and p.m. due to the prediction that C_{max} might exceed the exposure limits. Compound **9** was administered after 10 h of fasting in a 10, 50, and 100 mg powder-in-capsule formulation. The effect of food on the pharmacokinetics of **9** was evaluated at the 300 mg dose. Safety and tolerability were assessed by adverse event monitoring, laboratory values, and cardiovascular parameters including blood pressure, heart rate, and electrocardiogram.

The effects of **9** on inhibition of DNL and on whole-body fuel substrate utilization was assessed in a randomized, double-blinded, placebo-controlled crossover study in healthy volunteers (mean age 35.4 years [range 20−50 years]; mean body mass index (BMI) 29.9 kg/m^2; [range 25.8−35.5 kg/m^2]). Substrate utilization, assessed by RER, was measured in each of two study periods. Subjects were randomized to receive a single oral dose of **9** (600 mg) or placebo in the first period. In the second period, subjects were crossed over to receive the other treatment (placebo or **9**) at least 1 week apart. Oral fructose loading was used during the DNL and RER assessments to provide reproducible fractional contribution of DNL to VLDL-TG from one assessment period to the other.[31] A continuous infusion of ^{13}C-acetate (9−9.5 mg ^{13}C-acetic acid sodium salt per min via an infusion pump) was started at approximately 10:00 a.m. on the evening prior to each treatment period and continued until approximately 6:30 p.m. on the study day. Blood samples for assessment of the fractional contribution of DNL to VLDL-TG were collected and RER measures made hourly for 10 h. Subjects received study medication (**9** or matching placebo) at approximately 08:00 h (plus or minus 2 h). Subjects received a bolus of 0.25 g fructose/kg body weight every 30 min starting at approximately 08:30 h for approximately 9.5 h (total of 20 fructose administrations) during each of the two study periods. Urine samples for purpose of urinary nitrogen determination were collected during each study period. Subjects refrained from eating and drinking beverages other than water and the fructose drinks administered as part of study procedures. DNL was measured by ^{13}C-incorporation (derived from intravenous ^{13}C-acetate infusion) into VLDL palmitate using mass isotopomer distribution analysis (MIDA).[30] RER values reported are nonprotein RER as no changes in urinary nitrogen were observed during or between the study periods.

■ ASSOCIATED CONTENT

Supporting Information

In vitro characterization of **1m**, **4m**, and **9m**; enzymatic characterization of **9**. This material is available free of charge via the Internet at http://pubs.acs.org.

Accession Codes

PDB codes for human-yeast chimera acetyl CoA carboxylase CT domain bound to compounds **1** and **6** are 4WYO and 4WZ8, respectively.

■ AUTHOR INFORMATION

Corresponding Authors

*For D.A.G.: phone, 617-551-3287; E-mail, david.a.griffith@pfizer.com.

*For D.W.K.: phone, 860-715-1208; E-mail, daniel.w.kung@pfizer.com.

Notes

The authors declare the following competing financial interest(s): D.A.G., D.W.K., W.P.E., P.A.A., S.W.B., S.C.G., S.D.D., C.L., A.M.M., D.A.P., G.E.S., J.A.S., F.F.V. are employees of Pfizer Inc. ER is employed by Pennington Biomedical Research Center. CB and SMT are employed by KineMed, Inc.

■ ACKNOWLEDGMENTS

We are grateful to Scott Bader, Shawn Cabral, Carmen Garcia-Irizarry, Jana Polivkova, Colin Rose, and Derek Vrieze for synthesis of compounds; Kimberly Fennell, Alison Varghese, James Landro for protein generation and purification; Kristen Ford, Kristin Iamele Rockwell, and James Valentine for in vitro assays; Margaret Landis and Brenda Ramos for preclinical formulation assistance; David Beebe, Katherine Loomis, and Susan Tapley for in vitro and in vivo biology work; Mark Niosi and David Tess for drug metabolism studies and modeling; and Clare Buckeridge for analysis of human PK data. We thank Paul Dasilva-Jardine, Tim Rolph, and Sir Stephen O'Rahilly for helpful discussions. X-ray crystallographic data for this study were measured at beamline X29A of the National Synchrotron Light Source. Financial support comes principally from the Offices of Biological and Environmental Research and of Basic Energy Sciences of the U.S. Department of Energy, and from the National Center for Research Resources (P41RR012408) and the National Institute of General Medical Sciences (P41GM103473) of the National Institutes of Health. Use of the IMCA-CAT beamline 17-BM at the Advanced Photon Source was supported by the companies of the Industrial Macromolecular Crystallography Association through a contract with Hauptman−Woodward Medical Research Institute. Use of the Advanced Photon Source was supported by the U.S. Department of Energy, Office of Science, Office of Basic Energy Sciences, under contract no. DE-AC02-06CH11357. All studies were funded by Pfizer Inc.

■ ABBREVIATIONS USED

ACC, acetyl-CoA carboxylase; CL_{int}, intrinsic clearance; DNL, de novo lipogenesis; GCP, good clinical practice; HLM, human liver microsome; LipE, lipophilic efficiency; MCM, Modified Eagle Medium, Dr. Chee's Modification; MIDA, mass isotopomer distribution analysis; ND, not determined; QMCoA, quadriceps muscle malonyl-CoA; RER, respiratory exchange ratio; SBECD, sulfobutylether-β-cyclodextrin; SD, Sprague−Dawley

■ REFERENCES

(1) Saggerson, D. Malonyl-CoA, a key signaling molecule in mammalian cells. *Annu. Rev. Nutr.* **2008**, *28*, 253−272.

(2) Savage, D. B.; Petersen, K. F.; Shulman, G. I. Disordered lipid metabolism and the pathogenesis of insulin resistance. *Physiol. Rev.* **2007**, *87*, 507−520.

(3) Samuel, V. T.; Petersen, K. F.; Shulman, G. I. Lipid-induced insulin resistance: unravelling the mechanism. *Lancet* **2010**, *375*, 2267−2277.

(4) Harwood, H. J., Jr.; Petras, S. F.; Shelly, L. D.; Zaccaro, L. M.; Perry, D. A.; Makowski, M. R.; Hargrove, D. M.; Martin, K. A.; Tracey, W. R.; Chapman, J. G.; Magee, W. P.; Dalvie, D. K.; Soliman, V. F.; Martin, W. H.; Mularski, C. J.; Eisenbeis, S. A. Isozyme-nonselective N-substituted bipiperidylcarboxamide acetyl-CoA carboxylase inhibitors reduce tissue malonyl-CoA concentrations, inhibit fatty acid synthesis, and increase fatty acid oxidation in cultured cells and in experimental animals. *J. Biol. Chem.* **2003**, *278*, 37099−37111.

(5) Kotronen, A.; Seppala-Lindroos, A.; Vehkavaara, S.; Bergholm, R.; Frayn, K. N.; Fielding, B. A.; Yki-Jarvinen, H. Liver fat and lipid oxidation in humans. *Liver Int.* **2009**, *29*, 1439−1446.

(6) Tong, L.; Harwood, H. J., Jr. Acetyl-coenzyme A carboxylases: versatile targets for drug discovery. *J. Cell. Biochem.* **2006**, *99*, 1476−1488.

(7) Wang, C.; Rajput, S.; Watabe, K.; Liao, D. F.; Cao, D. Acetyl-CoA carboxylase-a as a novel target for cancer therapy. *Front. Biosci.* **2010**, *2*, 515−526.

(8) Gu, Y. G.; Weitzberg, M.; Clark, R. F.; Xu, X.; Li, Q.; Zhang, T.; Hansen, T. M.; Liu, G.; Xin, Z.; Wang, X.; Wang, R.; McNally, T.; Zinker, B. A.; Frevert, E. U.; Camp, H. S.; Beutel, B. A.; Sham, H. L. Synthesis and structure−activity relationships of *N*-{3-[2-(4-alkoxyphenoxy)thiazol-5-yl]-1- methylprop-2-ynyl}carboxy derivatives as selective acetyl-CoA carboxylase 2 inhibitors. *J. Med. Chem.* **2006**, *49*, 3770−3773.

(9) Gu, Y. G.; Weitzberg, M.; Clark, R. F.; Xu, X.; Li, Q.; Lubbers, N. L.; Yang, Y.; Beno, D. W.; Widomski, D. L.; Zhang, T.; Hansen, T. M.; Keyes, R. F.; Waring, J. F.; Carroll, S. L.; Wang, X.; Wang, R.; Healan-Greenberg, C. H.; Blomme, E. A.; Beutel, B. A.; Sham, H. L.; Camp, H. S. *N*-{3-[2-(4-Alkoxyphenoxy)thiazol-5-yl]-1-methylprop-2-ynyl}-carboxy derivatives as acetyl-coA carboxylase inhibitors—improvement of cardiovascular and neurological liabilities via structural modifications. *J. Med. Chem.* **2007**, *50*, 1078−1082.

(10) Glund, S.; Schoelch, C.; Thomas, L.; Niessen, H. G.; Stiller, D.; Roth, G. J.; Neubauer, H. Inhibition of acetyl-CoA carboxylase 2 enhances skeletal muscle fatty acid oxidation and improves whole-body glucose homeostasis in db/db mice. *Diabetologia* **2012**, *55*, 2044−2053.

(11) Keil, S.; Muller, M.; Zoller, G.; Haschke, G.; Schroeter, K.; Glien, M.; Ruf, S.; Focken, I.; Herling, A. W.; Schmoll, D. Identification and synthesis of novel inhibitors of acetyl-CoA carboxylase with in vitro and in vivo efficacy on fat oxidation. *J. Med. Chem.* **2010**, *53*, 8679−8687.

(12) Glien, M.; Haschke, G.; Schroeter, K.; Pfenninger, A.; Zoller, G.; Keil, S.; Muller, M.; Herling, A. W.; Schmoll, D. Stimulation of fat oxidation, but no sustained reduction of hepatic lipids by prolonged pharmacological inhibition of acetyl CoA carboxylase. *Horm. Metab. Res.* **2011**, *43*, 601−606.

(13) Kamata, M.; Yamashita, T.; Kina, A.; Funata, M.; Mizukami, A.; Sasaki, M.; Tani, A.; Funami, M.; Amano, N.; Fukatsu, K. Design, synthesis, and structure−activity relationships of novel spiro-piperidines as acetyl-CoA carboxylase inhibitors. *Bioorg. Med. Chem. Lett.* **2012**, *22*, 3643−3647.

(14) Kamata, M.; Yamashita, T.; Kina, A.; Tawada, M.; Endo, S.; Mizukami, A.; Sasaki, M.; Tani, A.; Nakano, Y.; Watanabe, Y.; Furuyama, N.; Funami, M.; Amano, N.; Fukatsu, K. Symmetrical approach of spiro-pyrazolidinediones as acetyl-CoA carboxylase inhibitors. *Bioorg. Med. Chem. Lett.* **2012**, *22*, 4769−4772.

(15) Bourbeau, M. P.; Siegmund, A.; Allen, J. G.; Shu, H.; Fotsch, C.; Bartberger, M. D.; Kim, K. W.; Komorowski, R.; Graham, M.; Busby, J.; Wang, M.; Meyer, J.; Xu, Y.; Salyers, K.; Fielden, M.; Veniant, M. M.; Gu, W. Piperazine oxadiazole inhibitors of acetyl-CoA carboxylase. *J. Med. Chem.* **2013**, *56*, 10132−10141.

(16) Schreurs, M.; van Dijk, T. H.; Gerding, A.; Havinga, R.; Reijngoud, D. J.; Kuipers, F. Soraphen, an inhibitor of the acetyl-CoA carboxylase system, improves peripheral insulin sensitivity in mice fed a high-fat diet. *Diabetes Obes. Metab.* **2009**, *11*, 987−991.

(17) Harriman, G.; Greenwood, J.; Bhat, S.; Tong, L.; Wang, R.; Paul, D.; Kapeller, R.; Harwood, H. J., Jr. Acetyl-CoA Carboxylase Inhibition by ND-630 Inhibits Fatty Acid Synthesis and Stimulates Fatty Acid Oxidation in Cultured Cells and in Experimental Animals. Poster session presented at Keystone Symposia Conference: Adipose Tissue Biology, Keystone, CO, January 27−February 1, 2013.

(18) Harriman, G.; Greenwood, J.; Bhat, S.; Kapeller, R.; Harwood, H. J., Jr. Acetyl-CoA Carboxylase Inhibition by ND-630 Inhibits Fatty Acid Synthesis, Stimulates Fatty Acid Oxidation, Reduces Body Weight, Improves Insulin Sensitivity, and Modulates Dyslipidemia in Rats. Poster session presented at American Diabetes Association Annual Meeting, Chicago, IL, June 21−25, 2013.

(19) Freeman-Cook, K. D.; Amor, P.; Bader, S.; Buzon, L. M.; Coffey, S. B.; Corbett, J. W.; Dirico, K. J.; Doran, S. D.; Elliott, R. L.; Esler, W.; Guzman-Perez, A.; Henegar, K. E.; Houser, J. A.; Jones, C. S.; Limberakis, C.; Loomis, K.; McPherson, K.; Murdande, S.; Nelson, K. L.; Phillion, D.; Pierce, B. S.; Song, W.; Sugarman, E.; Tapley, S.; Tu, M.; Zhao, Z. Maximizing lipophilic efficiency: the use of Free-Wilson analysis in the design of inhibitors of acetyl-CoA carboxylase. *J. Med. Chem.* **2012**, *55*, 935−942.

(20) Bagley, S. W.; Southers, J. A.; Cabral, S.; Rose, C. R.; Bernhardson, D. J.; Edmonds, D. J.; Polivkova, J.; Yang, X.; Kung, D. W.; Griffith, D. A.; Bader, S. J. Synthesis of 7-oxo-dihydrospiro-[indazole-5,4′-piperidine] acetyl-CoA carboxylase inhibitors. *J. Org. Chem.* **2012**, *77*, 1497−1506.

(21) Limberakis, C.; Li, J.; Balan, G.; Griffith, D. A.; Kung, D. W.; Rose, C.; Vrieze, D. Complementary α-alkylation approaches for a sterically hindered spiro[pyrazolopyranpiperidine]ketone. *Tetrahedron Lett.* **2012**, *53*, 2543−2547.

(22) Vickers, S.; Duncan, C. A.; Kari, P. H.; Homnick, C. F.; Elliott, J. M.; Pitzenberger, S. M.; Hichens, M.; Vyas, K. P. In vivo and in vitro metabolism studies on a class III antiarrhythmic agent. *Drug Metab. Dispos.* **1993**, *21*, 467−473.

(23) Details will be provided in a subsequent publication.

(24) Wong, J. M.; Mahon, W. A.; Kalow, W.; Inaba, T. Carbonyl (phenone) reductase in human liver: structure−activity relationship among substrates. *Drug Metab. Dispos.* **1992**, *20*, 465−466.

(25) Zhang, H.; Tweel, B.; Li, J.; Tong, L. Crystal structure of the carboxyltransferase domain of acetyl-coenzyme A carboxylase in complex with CP-640186. *Structure* **2004**, *12*, 1683−1691.

(26) Rajamohan, F.; Marr, E.; Reyes, A. R.; Landro, J. A.; Anderson, M. D.; Corbett, J. W.; Dirico, K. J.; Harwood, J. H.; Tu, M.; Vajdos, F. F. Structure-guided inhibitor design for human acetyl-coenzyme A carboxylase by interspecies active site conversion. *J. Biol. Chem.* **2011**, *286*, 41510−41519.

(27) Corbett, J. W.; Freeman-Cook, K. D.; Elliott, R.; Vajdos, F.; Rajamohan, F.; Kohls, D.; Marr, E.; Zhang, H.; Tong, L.; Tu, M.; Murdande, S.; Doran, S. D.; Houser, J. A.; Song, W.; Jones, C. J.; Coffey, S. B.; Buzon, L.; Minich, M. L.; Dirico, K. J.; Tapley, S.; McPherson, R. K.; Sugarman, E.; Harwood, H. J., Jr.; Esler, W.

Discovery of small molecule isozyme non-specific inhibitors of mammalian acetyl-CoA carboxylase 1 and 2. *Bioorg. Med. Chem. Lett.* **2010**, *20*, 2383−2388.
(28) Zhu, H.; Bakken, G. Water's Role in Compound Design for Drug Discovery. Poster session presented at Chemical Computing Group UGM & Conference, Montreal, Canada, June 27, 2013.
(29) Lombardo, F.; Shalaeva, M. Y.; Tupper, K. A.; Gao, F. ElogD(oct): a tool for lipophilicity determination in drug discovery. 2. Basic and neutral compounds. *J. Med. Chem.* **2001**, *44*, 2490−2497.
(30) Hellerstein, M. K. De novo lipogenesis in humans: metabolic and regulatory aspects. *Eur. J. Clin. Nutr.* **1999**, *53* (Suppl 1), S53−S65.
(31) Beysen, C.; Turner, S.; Carvajal-Gonzalez, S.; Buckeridge, C.; Hellerstein, M.; Esler, W. P.; Sonnenberg, G. E. A New Methodology for the Reproducible Measurement of Hepatic De Novo Lipogenesis in Humans. Poster session presented at American Diabetes Association Annual Meeting, San Francisco, CA, June 13−17, 2014.
(32) Bagley, S. W.; Griffith, D. A.; Kung, D. W.-S. N1-pyrazolospiroketone acetyl-CoA carboxylase inhibitors. U.S. Patent 8 288 405 B2, 2012.
(33) Kabsch, W. XDS. *Acta Crystallogr., Sect. D: Biol. Crystallogr.* **2010**, *66*, 125−132.
(34) Vonrhein, C.; Flensburg, C.; Keller, P.; Sharff, A.; Smart, O.; Paciorek, W.; Womack, T.; Bricogne, G. Data processing and analysis with the autoPROC toolbox. *Acta Crystallogr., Sect. D: Biol. Crystallogr.* **2011**, *67*, 293−302.
(35) Evans, P. Scaling and assessment of data quality. *Acta Crystallogr., Sect. D: Biol. Crystallogr.* **2006**, *62*, 72−82.
(36) French, S.; Wilson, K. On the Treatment of Negative Intensity Observations. *Acta Crystallogr., Sect. A: Found. Crystallogr.* **1978**, *A34*, 517−525.
(37) Winn, M. D.; Ballard, C. C.; Cowtan, K. D.; Dodson, E. J.; Emsley, P.; Evans, P. R.; Keegan, R. M.; Krissinel, E. B.; Leslie, A. G. W.; McCoy, A.; McNicholas, S. J.; Murshudov, G. N.; Pannu, N. S.; Potterton, E. A.; Powell, H. R.; Read, R. J.; Vagin, A.; Wilson, K. S. Overview of the CCP4 suite and current developments. *Acta Crystallogr., Sect. D: Biol. Crystallogr.* **2011**, *67*, 235−242.
(38) *BUSTER*, version 2.9.5; Global Phasing Ltd.: Cambridge, United Kingdom, 2011).
(39) Murshudov, G. N.; Vagin, A. A.; Dodson, E. J. Refinement of Macromolecular Structures by the Maximum-Likelihood Method. *Acta Crystallogr., Sect. D: Biol. Crystallogr.* **1997**, *D53*, 240−255.
(40) Kim Fennell and Alison Varghese, personal communication.